Journal of Medicinal Chemistry

pubs.acs.org/jmc

Article

Novel Biphenyl Pyridines as Potent Small-Molecule Inhibitors Targeting the Programmed Cell Death-1/Programmed Cell Death-Ligand 1 Interaction

Tianyu Wang, Shi Cai, Mingming Wang, Wanheng Zhang, Kuojun Zhang, Dong Chen, Zheng Li, and Sheng Jiang*

Cite This: *J. Med. Chem.* 2021, 64, 7390−7403

Read Online

ACCESS | Metrics & More | Article Recommendations | Supporting Information

ABSTRACT: With the successful clinical application of anti-programmed cell death-1 (PD-1)/programmed cell death-ligand 1 (PD-L1) monoclonal antibodies (mAb), targeting the PD-1/PD-L1 interaction has become a promising method for the discovery of cancer therapy. Due to the inherent limitations of antibodies, it is necessary to search for small-molecule inhibitors against the PD-1/PD-L1 axis. We report the design, synthesis, and evaluation *in vitro* and *in vivo* of a series of novel biphenyl pyridines as the inhibitors of PD-1/PD-L1. 2-(((2-Methoxy-6-(2-methyl-[1,1′-biphenyl]-3-yl)-pyridin-3-yl)methyl)amino)ethan-1-ol (**24**) was found to inhibit the PD-1/PD-L1 interaction with an IC_{50} value of 3.8 ± 0.3 nM and enhance the killing activity of tumor cells by immune cells. Compound **24** displays great pharmacokinetics (oral bioavailability of 22%) and significant *in vivo* antitumor activity in a CT26 mouse model. Flow cytometry and immunohistochemistry data indicated that compound **24** activates the immune activity in tumors. These results suggest that compound **24** is a promising small-molecule inhibitor against the PD-1/PD-L1 axis and merits further development.

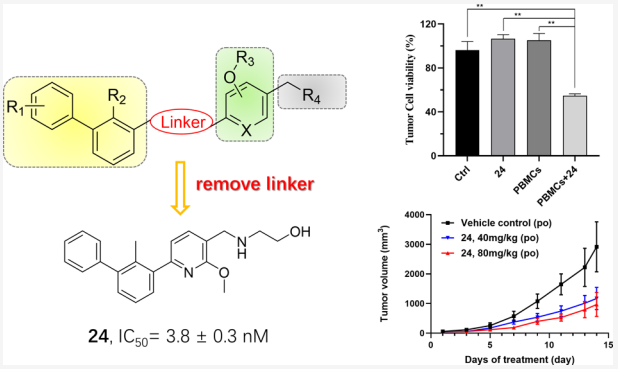

INTRODUCTION

Tumor cells hijack certain immune checkpoint pathways to suppress the activation of immune cells and thus evade immune surveillance.[1−3] The blockade of immune checkpoint pathways by specific inhibitors can restore or increase the antitumor immunity of the body.[4,5] With the recent clinical success of immune checkpoint inhibitors in cancer patients, the method has become an important branch of cancer therapy.[6−8] Blockade of programmed cell death-1 (PD-1) and its ligand−−programmed cell death-ligand 1 (PD-L1) has achieved the most remarkable clinical success, and this work was awarded the Nobel Prize in Physiology or Medicine in 2018.[9,10] PD-1, also known as CD279, is a homologue of CD28 consisting of 288 amino acids. It is expressed on the surface of many types of immune cells and is upregulated in activated T cells.[11,12] The interaction of PD-1 with its ligand PD-L1 (also known as B7−H1 or CD274) impedes T cell receptor-mediated signaling and induces T cell anergy and functional exhaustion.[13,14] Under normal physiological conditions, the PD-1/PD-L1 pathway provides inhibitory signals to maintain self-tolerance and protect tissues from the damage of excessive immune responses. However, the aberrant expression of PD-L1 on the surface of several types of tumor cells, such as esophageal cancer, pancreatic cancer, and breast cancer cells, interacts with PD-1 on T cells to evade immune surveillance.[2,15]

Currently, the US Food and Drug Administration (FDA) has approved six monoclonal antibodies (mAbs) of the PD-1/PD-L1 pathway, including three PD-1 inhibitors (nivolumab, pembrolizumab, and cemiplimab) and three PD-L1 inhibitors (atezolizumab, durvalumab, and avelumab). Both anti-PD-1 and anti-PD-L1 mAbs exhibit promising clinical antitumor activity in the treatment of melanoma, non-small-cell lung cancer, and urothelial carcinoma.[16] However, mAbs targeting the PD-1/PD-L1 pathway have several disadvantages including their long half-life, unchecked immune response, and immune-related adverse events.[17] Moreover, lack of oral bioavailability and poor permeability of tumor tissues are the disadvantages of PD-1/PD-L1 therapeutic antibodies used in clinics. A promising alternative to overcome these limitations is the

Received: January 4, 2021
Published: May 31, 2021

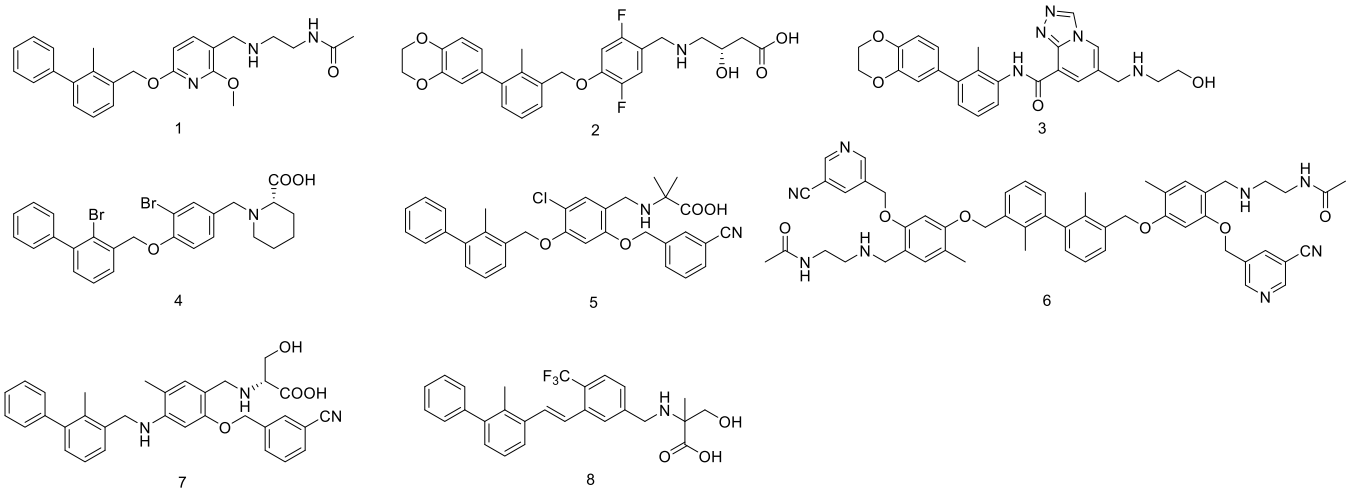

Figure 1. Chemical structures of the reported small-molecule inhibitors targeting the PD-1/PD-L1 pathway.

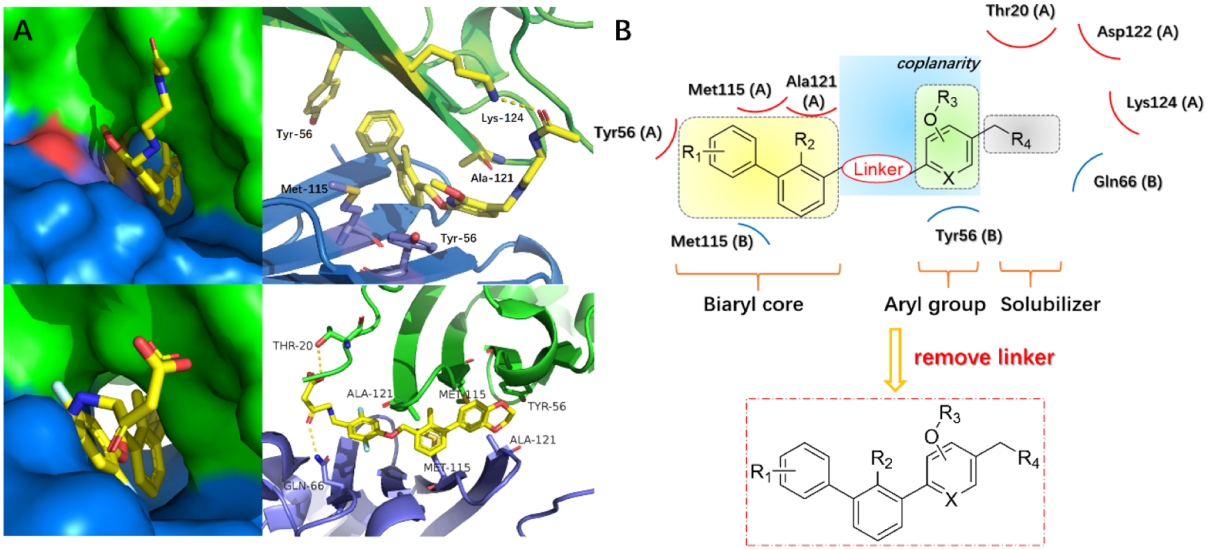

Figure 2. (A) Crystal structure of the PD-L1/**1** complex (above, PDB code 5J89) and PD-L1/**2** (below, PDB code 5N2F); chain A, green; chain B, blue; hydrogen bonds are shown as yellow dashed lines; (B) pharmacophoric model and design strategy of compounds.

application of small-molecule inhibitors of the PD-1/PD-L1 pathway.[18]

During the past few years, small-molecule inhibitors targeting the PD-1/PD-L1 pathway have made substantial progress.[19] The crystal structures of the human PD-1/PD-L1 complex and small molecules complexed with PD-L1 have been disclosed, and the small-molecule interaction "hot spots" on PD-L1 have been identified.[20−22] To date, several potent small-molecule inhibitors targeting PD-L1 have been reported (Figure 1).[23−28] The analysis of the crystal structures of the PD-L1/inhibitor complex suggests that an aromatic ring system is the core pharmacophore for PD-L1 binding, but to date, no small-molecule inhibitors targeting the PD-1/PD-L1 pathway have been approved for cancer treatment, and the development of marketable inhibitors for clinics remains a challenging process. In the future, the search for novel small-molecule inhibitors targeting the PD-1/PD-L1 pathway with more structural diversity, high potency, and further investigative data *in vitro* and *in vivo* will continue in drug development.

In the present study, we designed and synthesized novel biphenyl pyridines as potent small-molecule inhibitors of the PD-1/PD-L1 pathway. We evaluated their biochemical activities and investigated the preliminary structure−activity relationships (SARs). According to detailed structural modifications, compound **24** was identified as the most potent inhibitor with an IC_{50} of 3.8 ± 0.3 nM, as assessed by a time-resolved fluorescence resonance energy transfer (TR-FRET) assay. Compound **24** remarkably activates the antitumor activities of human peripheral blood mononuclear cells (PBMC) which kill MDB-MB 231 cells. *In vivo*, compound **24**, administered orally, significantly inhibits tumor growth in a CT26 mouse model and displays significant activation of the immune microenvironment in the tumor.

RESULTS AND DISCUSSION

Drug Design and Chemical Synthesis. As shown in Figure 2A, compounds **1** and **2** insert into a deep cylindrical and hydrophobic pocket at the interface of the PD-L1 dimer. The distal phenyl ring within the biphenyl core creates a T-stacking interaction with $_A$Tyr56, and the phenylmethyl ring

https://doi.org/10.1021/acs.jmedchem.1c00010
J. Med. Chem. 2021, 64, 7390−7403

Scheme 1. Synthesis of Compounds 15−17[a]

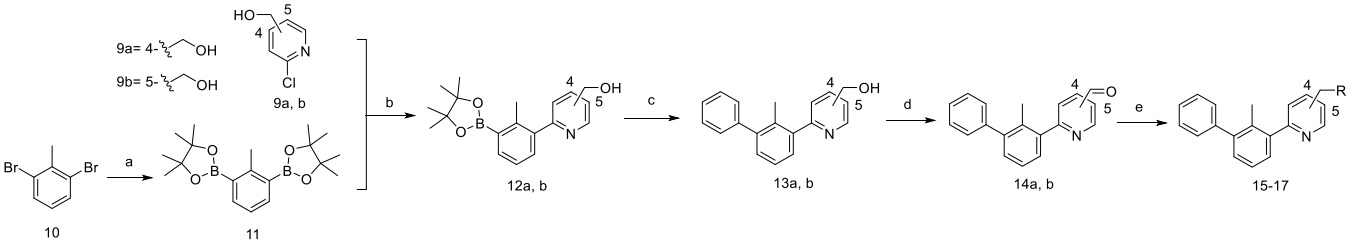

[a]Reagents and conditions: (a) Bis(pinacolato)diboron, $PdCl_2$(dppf), KOAc, 1,4-dioxane, 130 °C, overnight; (b) $Pd(PPh_3)_4$, K_2CO_3, 1,4-dioxane/H_2O (10:1), 85 °C, 4 h; (c) XPhos Pd G2, K_3PO_4, bromobenzene, THF/H_2O (3:1), 80 °C, overnight; (d) DMP, $NaHCO_3$, DCM/DMF (4/1), rt, 0.5 h; (e) appropriate amine, HOAc, $NaBH_3CN$, CH_3OH/CH_2Cl_2 (1:1), rt, 6−10 h.

Scheme 2. Synthesis of Compounds 24−40 and 43[a]

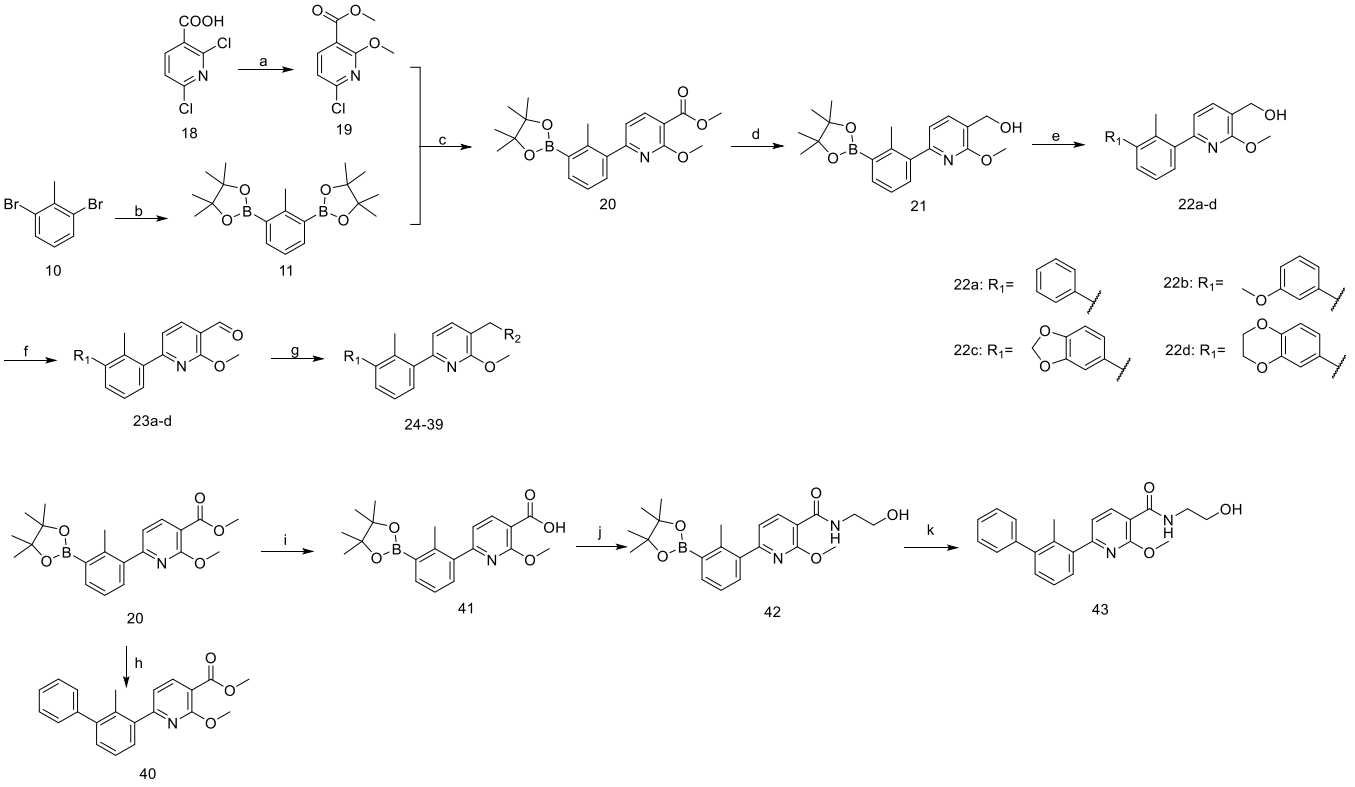

[a]Reagents and conditions: (a) MeOH, NaH, THF, 60 °C, 2 h; $SOCl_2$, MeOH, 70 °C, 3 h; (b) bis(pinacolato)diboron, $PdCl_2$(dppf), KOAc, 1,4-dioxane, 130 °C, overnight; (c) $Pd(PPh_3)_4$, K_2CO_3, 1,4-dioxane/H_2O (10:1), 85 °C, 4 h; (d) $LiAlH_4$, THF, rt, 3 h; (e) XPhos Pd G2, K_3PO_4, R_1Br, THF/H_2O (3:1), 80 °C, overnight; (f) DMP, $NaHCO_3$, DCM/DMF (4/1), room temperature (rt), 0.5 h; (g) appropriate amine, HOAc, $NaBH_3CN$, CH_3OH/CH_2Cl_2 (1:1), rt, 6−10 h; (h) XPhos Pd G2, K_3PO_4, bromobenzene, THF/H_2O (3:1), 80 °C; (i) LiOH, MeOH/THF/H_2O; (j) 2-aminoethanol, HOBT, EDCI, CH_2Cl_2; (k) XPhos Pd G2, K_3PO_4, bromobenzene, THF/H_2O (3:1), 80 °C, overnight.

enjoys a hydrophobic interaction with $_A$Ala121, $_A$Met115, and $_B$Met115. The aryl group is involved in $\pi-\pi$ stacking with $_B$Tyr56. In order to support the molecule being inserted into this deep cylindrical cavity, the linker, which links the phenylmethyl and aryl groups, must be approximatively coplanar with the aryl group. The solubilizer R_4 at the distal end stretches out of the cavity into the solvent and may interact with PD-L1 through hydrogen bonds. Most reported inhibitors appear to follow the pharmacophoric model shown in Figure 2B. Among the reported inhibitors in Figure 1, ethers and amides are commonly chosen as the linkers, which are replaceable and play a limited role in SARs. Accordingly, we designed biphenyl pyridines as novel small-molecule inhibitors, as shown in Figure 2B. We abandoned the original linker and instead linked the aryl group and biaryl core directly. With the direct coupling of the aryl and phenylmethyl groups, the aryl group will provide additional hydrophobic interaction with $_A$Ala121 and $_A$Met115. Being directly connected with the phenylmethyl unit, the aryl group can rotate through various angles, and this allows it to interact more easily with $_B$Tyr56 through $\pi-\pi$ stacking.

The synthesis of biphenyl pyridines **15−17** is described in Scheme 1. The preparation of 2,2′-(2-methyl-1,3-phenylene)-bis(4,4,5,5-tetramethyl-1,3,2-dioxaborolane) (**11**) was accomplished by borylation of the commercially available 1,3-dibromo-2-methylbenzene (**10**). Compound **11** reacted with **9a** or **9b** under Suzuki−Miyaura coupling conditions to afford the intermediate **12a** or **12b**, respectively. Suzuki−Miyaura

https://doi.org/10.1021/acs.jmedchem.1c00010
J. Med. Chem. 2021, 64, 7390−7403

coupling of **12a** or **12b** with bromobenzene yielded **13a** or **13b**. Then, **13a** or **13b** was oxidized to aldehydes **14a** or **14b** by Dess−Martin periodinane. Finally, the target compounds **15**−**17** were generated by reductive amination using $NaBH_3CN$ and the appropriate amines.

The synthesis of biphenyl pyridine compounds **24**−**40** and **43** is shown in Scheme 2. The methylation and methyl ester formation of the commercially available 2,6-dichloronicotinic acid led to the formation of intermediate **19**. Compound **20** was generated from **11** and **19** using the Suzuki−Miyaura coupling reaction. Using $LiAlH_4$, **20** was reduced to alcohol (**21**). **21** reacted with phenylboronic acid or a substituted phenylboronic acid and yielded **22a**−**22d**. By adopting synthetic routes similar to those used for **15**−**17**, target compounds **24**−**39** were generated. Compound **40** was produced by Suzuki−Miyaura coupling of **20** with bromobenzene. Compound **43** was generated from intermediate **20** by hydrolysis and subsequent acylation.

Biochemical Evaluation and Structure Optimization. Initially, compounds **15**−**17**, **24**, and **25** were synthesized in an effort to validate our design strategy. The activities of inhibitors targeting the PD-1/PD-L1 pathway were evaluated by using the well-established TR-FRET assay. The resulting IC_{50} values are presented in Table 1. As shown in Table 1, biphenyl

Table 1. SARs of Compounds 15−17, 24, and 25 by PD-1/PD-L1 TR-FRET Assay

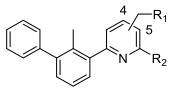

15-17, 24, 25

Compound	R_1	R_2	PD-1/PD-L1 IC_{50} (nM)[a]
1	/	/	14.9 ± 1.8
15		H	130.6 ± 9.6
16		H	34.6 ± 2.4
17	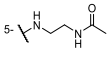	H	52.8 ± 5.2
24			3.8 ± 0.3
25	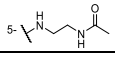		14.4 ± 1.2

[a]The data are displayed as averages of duplicate assays ± SD.

pyridine compounds **15**−**17** exhibited excellent inhibitory activities against the PD-1/PD-L1 interaction, with IC_{50} values of 130.6 ± 9.6, 34.6 ± 2.4, and 52.8 ± 5.2 nM, respectively. Comparisons of **15** with **16** and **17** indicated that shifting the solubilizing tail of biphenyl pyridines from the 4- to the 5-position led to obviously increased activity. When a methoxy group was introduced to the pyridine ring, sharply increased activities of compounds **24** and **25** were observed, indicating that methoxy attached to the pyridine is beneficial. Compound **24** displayed potent activity, with an IC_{50} value of 3.8 ± 0.3 nM, approximately 4 times that of the activity of the positive compound (**1**). Preliminary biochemical evaluation demonstrated that biphenyl pyridine compounds lacking a linker exhibited improved activity over that of the reported inhibitors of the PD-1/PD-L1 pathway. This is consistent with the pharmacophoric model in Figure 2B.

In view of the excellent activity of compound **24**, the alkoxypyridine fragment was retained, and further modifications were conducted by replacing the solubilizer tail on the pyridine. A series of hydrophilic moieties were introduced, yielding compounds **26**−**32**, as shown in Table 2. All the

Table 2. SARs of Compounds 26−32 by PD-1/PD-L1 TR-FRET Assay

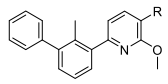

26-32

Compound	R	PD-1/PD-L1 IC_{50} (nM)[a]
26		17.0 ± 1.8
27	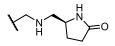	14.2 ± 2.8
28		8.4 ± 1.2
29		5.0 ± 0.2
30	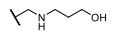	7.4 ± 0.5
31		8.5 ± 1.1
32		20.8 ± 1.6
1	/	14.9 ± 1.8

[a]The data are displayed as averages of duplicate assays ± SD.

biphenyl alkoxypyridine compounds (**24**−**32**) displayed promising activities against the PD-1/PD-L1 interaction, with almost all the IC_{50} values below 20 nM, again demonstrating the potent efficacy of biphenyl pyridines as PD-1/PD-L1 inhibitors. Among these, compounds **24** and **28**−**31**, containing an alcohol group, showed somewhat better inhibitory activities of PD-1/PD-L1, with IC_{50} values below 10 nM. Optimization of the tail group indicated that the solubilizer tail containing a hydroxyl group may contribute more hydrogen bond-like interactions with PD-L1.

In further investigations, compounds **33**−**35** which have diverse extensions of the distal phenyl ring within the biphenyl core were synthesized. In view of the T-stacking interaction with $_A$Tyr56, we chose a suitable substituent that can maintain this interaction. As shown in Table 3, compounds **33**−**35** displayed good inhibition of the PD-1/PD-L1 interaction, and compound **35** with 2,3-dihydro-1,4-benzodioxinyl moiety showed better activity (IC_{50}, 7.9 ± 1.1 nM). However, all these compounds exhibited lower activities than the precursor compound **24**. Because the introduction of the 2,3-dihydro-1,4-benzodioxinyl moiety facilitated the binding pocket of PD-L1 as a deep, enlarged hydrophobic tunnel, we further investigated the activity of 2,3-dihydro-1,4-benzodioxinyl analogues. Compared with the biphenyl compounds **25**, **26**, **30**, and **32**, compounds **36**−**39** exhibited almost equal inhibitory activity, as shown in Table 3, but **24** was still the most potent compound. Replacement of the aminoethanol group of compound **24** with a methyl ester and reaction with *N*-(2-hydroxyethyl)acetamide yielded compounds **40** and **43**, which had however sharply decreased activities, with the IC_{50} values of 326.1 ± 18.5 and 327 ± 12.1 nM, respectively.

https://doi.org/10.1021/acs.jmedchem.1c00010
J. Med. Chem. 2021, 64, 7390−7403

Table 3. SARs of Compounds 33−40 and 43 by PD-1/PD-L1 TR-FRET Assay

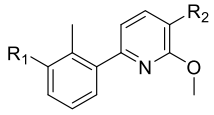

Compound	R_1	R_2	PD-1/PD-L1 IC_{50} (nM)[a]
33			12.6 ± 1.5
34			13.2 ± 1.8
35			7.9 ± 1.1
36		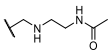	14.1 ± 0.2
37			10.4 ± 0.4
38			16.7 ± 0.9
39		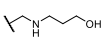	7.7 ± 0.2
40			326.1 ± 18.5
43			327 ± 12.1
1	/	/	14.9 ± 1.8

[a]The data are displayed as averages of duplicate assays ± SD.

Docking Analysis of Compound 24 with the PD-L1 Dimer. To investigate the binding mode of biphenyl pyridine compounds with the PD-L1 dimer, an analysis of the docking of compound **24** with dimeric PD-L1 was conducted. The docking results showed that **24** entered into the deep hydrophobic cleft formed by dimeric PD-L1 (Figure 3). Consistent with the binding mode of compounds **1** and **2** with PD-L1, the distal phenyl creates a T-stacking interaction with $_A$Tyr56, and the phenylmethyl provides hydrophobic interactions with $_A$Ala121, $_A$Met115, and $_B$Met115. As anticipated, the pyridine group, linking to phenylmethyl directly without a linker, participated in $\pi-\pi$ stacking with $_B$Tyr56 and in hydrophobic interactions with $_A$Ala121, providing a strong stabilization of the binding with the PD-L1 dimer. The aminoethanol tail of **24** interacts with $_A$Asp122 and $_B$Gln66 via two hydrogen bonds and contributes to the high binding affinity to dimeric PD-L1.

Antitumor Immunity of PBMCs Activated by Compound 24. To evaluate the potency of compound **24** inducing antitumor immunity, we investigated the effects of compound **24** on the killing of MDB-MB 231 cells by human PBMC. Tumor cell viability was detected by the lactate dehydrogenase (LDH) release. As shown in Figure 4, compound **24** at a concentration of 1.5 μM is not toxic toward MDB-MB 231 cells, and PBMCs alone failed to show antitumor activity to MDB-MB 231 cells. When PBMCs were incubated with different concentrations of compound **24**, dead tumor cells were produced by the treatment with PBMCs and **24**. Compound **24** significantly activated the antitumor immunity of PBMCs in a dose-dependent manner, with the estimated EC_{50} value of ∼100 nM. Dead tumor cells increased upon

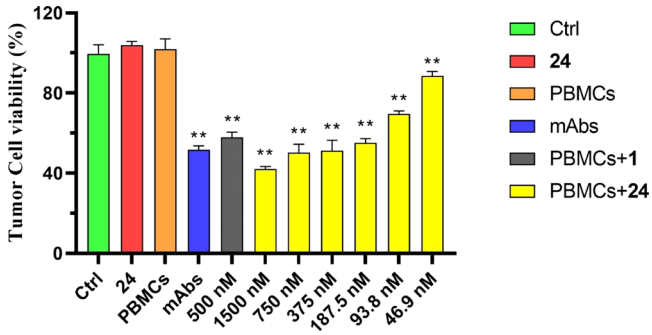

Figure 4. Compound **24** enhances the killing by PBMCs of MDA-MB-231 cells. Tumor cell viability was detected by LDH release at MDA-MB-231 cells/PBMCs (1:10). All data are presented as mean ± SD, $^{**}P < 0.05$ vs PBMC group, $n = 3$.

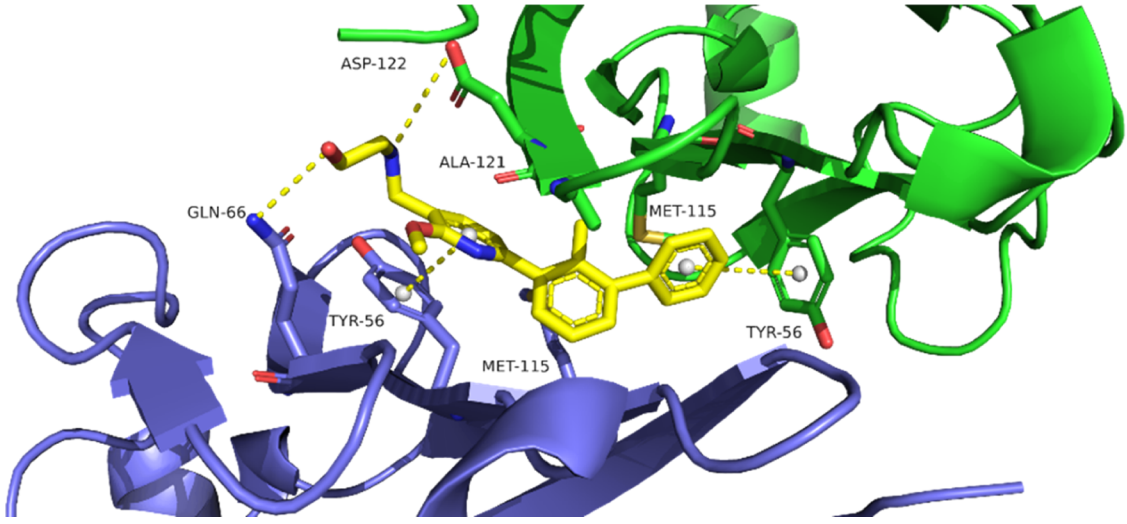

Figure 3. Docking analysis of compound **24** with the PD-L1 dimer (chain A, green; chain B, blue). The PDB code for the dimeric PD-L1 protein is 5J89.

https://doi.org/10.1021/acs.jmedchem.1c00010
J. Med. Chem. 2021, 64, 7390−7403

treatment with 375 nM compound **24** (53%), which is higher than 5 μg/mL durvalumab (49%) and 500 nM compound **1** (44%).

***In Vivo* Pharmacokinetic Properties of Compound 24.** We further evaluated the pharmacokinetic (PK) properties of compound **24** in Sprague-Dawley (SD) rats. The primary PK parameters of compound **24** via intravenous (iv) and oral (per os, po) routes are shown in Table 4. After the iv administration of compound **24** (3 mg/kg), the values of $AUC_{(0-t)}$ and C_{max} of compound **24** are 430.5 ± 49.8 ng/mL·h and 1233 ± 461.7 ng/mL, respectively. The plasma clearance (Cl) and half-life ($t_{1/2}$) of compound **24** are 11.5 ± 1.1 L/h/kg and 4.2 ± 1.6 h, respectively. When compound **24** was administrated orally (25 mg/kg), the half-life ($t_{1/2}$) of compound **24** reached 6.4 ± 2.8 h. Moreover, compound **24** exhibited markedly excellent oral exposure, with oral bioavailability (F) of 22%. These results indicated that compound **24** exhibited good PK properties and excellent potency of oral administration, which are rarely seen in the reported small-molecule inhibitors targeting the PD-1/PD-L1 pathway in Figure 1.

Table 4. Primary PK Parameters of Compound 24 in SD Rats

PK parameters[a]	iv (3 mg/kg)	po (25 mg/kg)
$AUC_{(0-t)}$ (ng/mL·h)	430.5 ± 49.8	787.4 ± 103.5
C_{max} (ng/mL)	1233 ± 461.7	192.0 ± 87.8
$t_{1/2}$ (h)	4.2 ± 1.6	6.4 ± 2.8
T_{max}	0.03	0.69 ± 1.1
Cl (L/h/kg)	11.5 ± 1.1	28.8 ± 6.6
V_z (L/kg)	78.6 ± 41.0	249.3 ± 66.5
F (%)		22

[a]AUC, area under the curve; $t_{1/2}$, half-life; T_{max}, time of maximum plasma concentration; C_{max}, maximum plasma concentration; Cl, plasma clearance; V_z, apparent distribution volume; F, oral bioavailability. n = 4, mean ± SD.

***In Vivo* Antitumor Activity of Compound 24.** To assess the antitumor activity of compound **24**, we evaluated its *in vivo* antitumor efficacy using a CT26 mouse model in BALB/c mice. After the tumor volume reached approximately 50 mm^3, the mice were treated either with a vehicle control or with compound **24** (40, 80 mg/kg) by oral administration once a day for 2 weeks. The results of tumor growth inhibition (TGI) in different groups at different days after treatment are shown in Figure 5A. Compound **24** inhibited tumor growth in a dose-dependent manner and did not cause any body weight loss or mortality during treatment (Figure 5B), indicating that all doses of **24** were well tolerated. Based on the final tumor weights, groups treated with compound **24** were significantly superior to those treated with the vehicle control (Figure 5C,D). Doses of 40 and 80 mg kg^{-1} day^{-1} significantly decreased the final tumor weight, with TGI values of 60 and 67%, respectively, compared with an untreated vehicle group. These results confirmed the efficacy of compound **24** *in vivo* as an oral small-molecule inhibitor of the PD-1/PD-L1 pathway.

Dissociated tumors were digested into single cells and analyzed with flow cytometry after being dyed with different tumor-infiltrating lymphocyte (TIL) markers. As shown in Figure 6A,B, the level of cytotoxic T cells ($CD8^+$ cells) in tumor tissue increased distinctly after treatment with compound **24** in a dose-dependent manner, when compared to the vehicle control group. When treated with compound **24**, the ratio of $CD4^+/CD8^+$ cells was obviously less than that in the vehicle control (Figure 6C). We also analyzed tumor

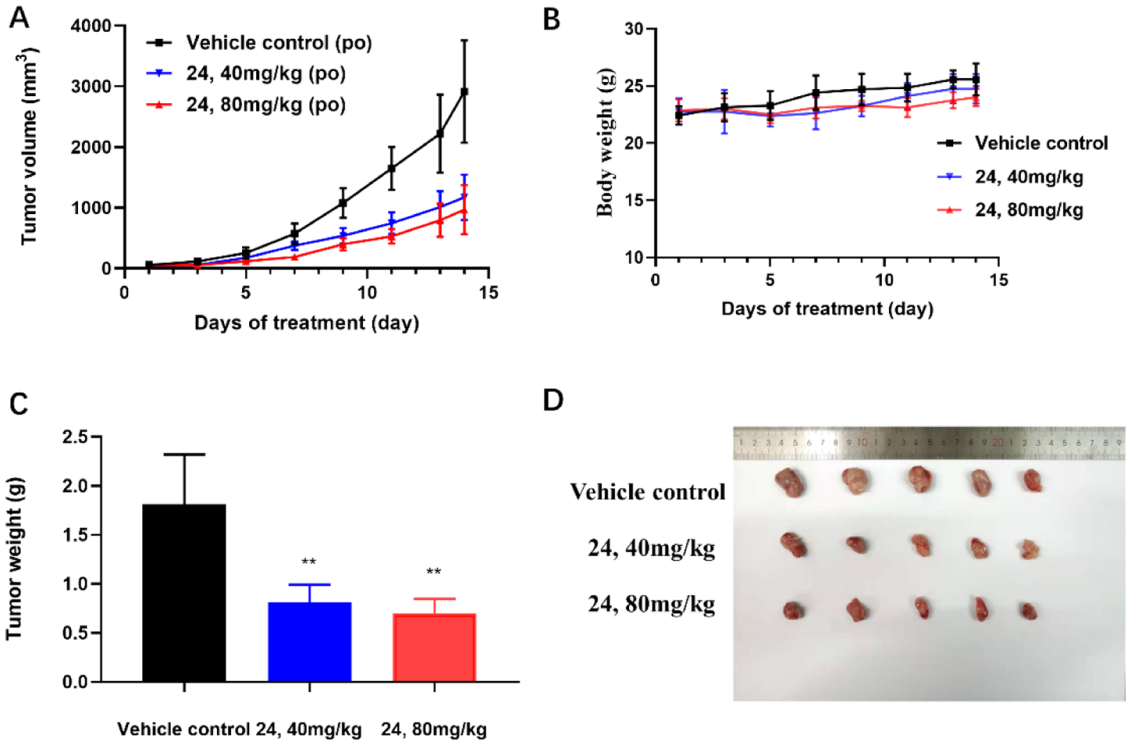

Figure 5. *In vivo* antitumor activity of compound **24** against CT26 tumor in mice. (A) Tumor volume changes during treatment. (B) Body weight changes of mice during treatment. (C) Weight of the excised tumors of each group. (D) Image of the excised tumors in each group after treatment. All data are presented as mean ± SD, $^{**}P < 0.05$ vs control group, n = 5.

https://doi.org/10.1021/acs.jmedchem.1c00010
J. Med. Chem. 2021, 64, 7390−7403

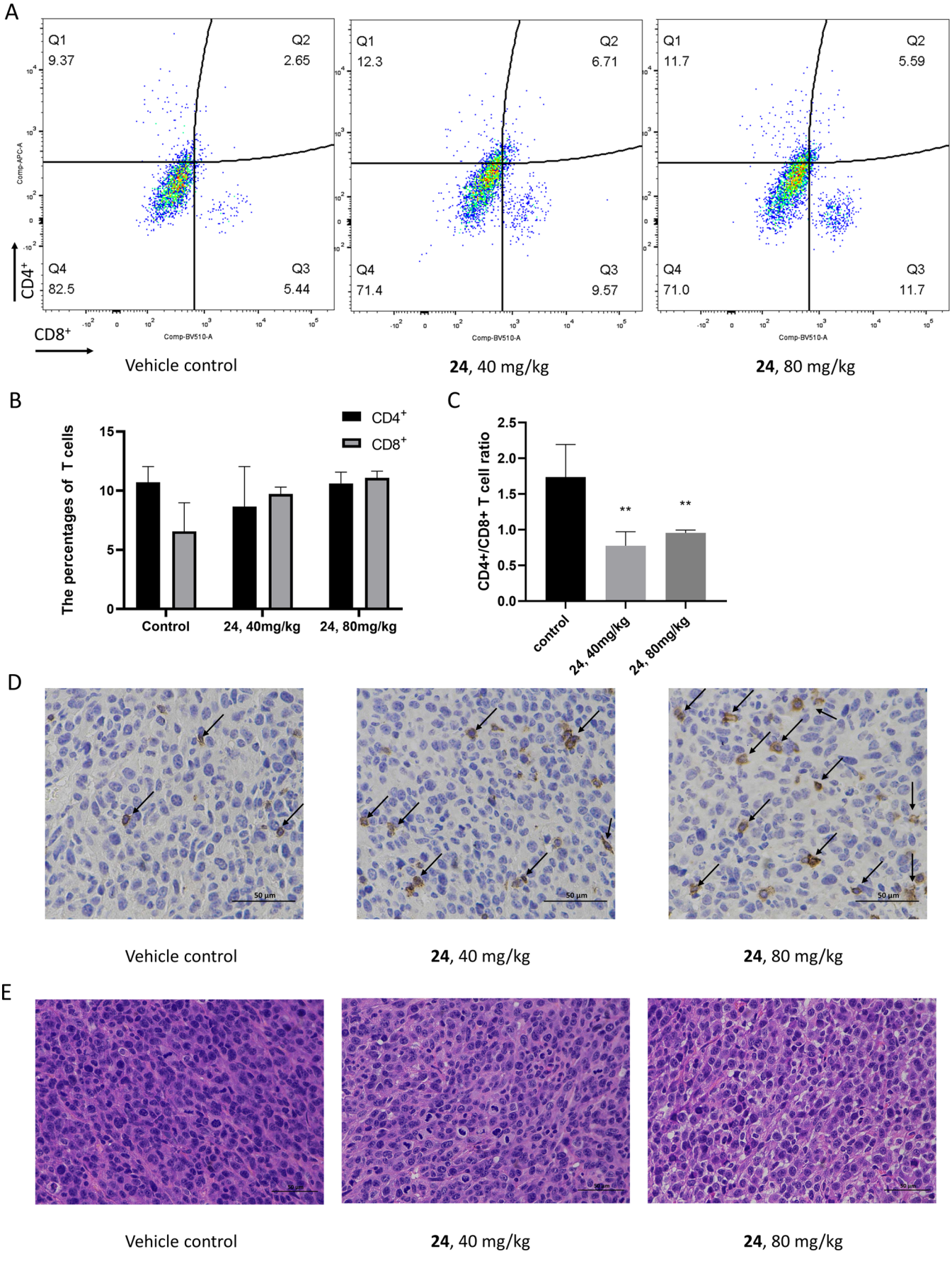

Figure 6. (A) Representative examples for $CD4^+$ and $CD8^+$ cells in dissociated tumors of vehicle control or mice treated with compound **24**. (B) Percentage of $CD4^+$ and $CD8^+$ cells in $CD3^+$ cells of tumor tissue. (C) Ratio of $CD4^+/CD8^+$ cells of tumor tissue. All data are presented as mean ±

https://doi.org/10.1021/acs.jmedchem.1c00010
J. Med. Chem. 2021, 64, 7390−7403

Figure 6. continued

SD, $^{**}P < 0.05$ vs control group, $n = 3$. (D) Representative immunohistochemistry determination of $CD8^+$ cell infiltration into tumor tissues. Scale bars, 50 μM. (E) H&E staining of tumor tissues. Scale bars, 50 μM.

tissues by immunohistochemistry. In agreement with the results of flow cytometry, significant increased infiltration of $CD8^+$ cells was observed in tumor tissues treated with compound **24**, compared with those treated with the vehicle control (Figure 6D). Hematoxylin and eosin (H&E) staining of tumor tissues revealed that tumor cells treated with **24** had decreased nucleus-to-cytoplasm ratios, and compound **24** induced tumor shrinkage and inhibited tumor cell growth (Figure 6E). These data demonstrated that compound **24** enhances the infiltration of $CD8^+$ cells and activated immune activity in tumors.

We further directly compared the *in vivo* antitumor efficacy of compound **24** with the reported PD-L1 inhibitor compound **1** and antimouse PD-L1 antibody using a CT26 mouse model in BALB/c mice. As shown in Figure S1, at the same dose and mode of administration (40 mg/kg, orally), compound **24** (TGI = 57%) showed obviously better TGI compared with compound **1** (TGI = 32%). Moreover, compound **24** showed better *in vivo* activity than PD-L1 antibody (TGI = 45%). Overall, compound **24** exhibited excellent TGI, administered orally, comparable to PD-L1 antibody, and demonstrated significantly higher *in vivo* activity than the previously described PD-L1 inhibitor compound **1**.

CONCLUSIONS

Along with the successful clinical application of anti-PD-1/PD-L1 mAbs, immune checkpoint inhibitors against PD-1/PD-L1 interaction have made them a promising target for cancer therapy. Although anti-PD-1/PD-L1 mAbs have gained a large market share, lack of oral bioavailability, emergence of tumor resistance, and difficult and expensive production of the mAbs also limit their current clinical application. In contrast, small molecules in general are more accessible and have higher oral bioavailability and acceptable half-lives. Consequently, the development of small-molecule inhibitors of PD-1/PD-L1 interaction is a promising alternative to mAbs.

We designed and synthesized a series of biphenyl pyridines as novel inhibitors of the PD-1/PD-L1 interaction. This novel chemical series showed great inhibitory activity of the PD-1/PD-L1 blockage in the TR-FRET assay. Among them, compound **24** was the most promising small-molecule inhibitor, with the IC_{50} value of 3.8 ± 0.3 nM. A PBMC killing assay indicated that **24** could activate the antitumor immunity of T cells in PBMCs. Compound **24** exhibited favorable PK properties with excellent oral bioavailability. Orally administered compound **24** significantly inhibits tumor growth in the CT26 mouse model. In addition, flow cytometry and immunohistochemistry demonstrated that **24** enhances immune activity in tumors. Compared with the reported PD-L1 inhibitors in Figure 1, compound **24** exhibited better *in vitro* inhibitory activity against PD-1/PD-L1 interaction and demonstrated significantly improved potency of oral administration and *in vivo* antitumor activity, which also indicated its potency and advantages as an alternative to mAbs. Overall, our work has demonstrated that **24** has the potential to serve as a lead compound for further novel small-molecule inhibitors of the PD-1/PD-L1 system.

EXPERIMENTAL SECTION

General Methods. Reagents and solvents were obtained from commercial sources and used without further purification. All reactions were carried out in oven-dried glassware. ^{1}H NMR and ^{13}C NMR spectra were recorded on Bruker AV-400 or Bruker AV-500 spectrometers, with TMS as an internal standard. Low-resolution ESI-MS spectra were recorded on an Agilent 1100 LC−MS spectrometer. High-resolution mass (HRMS) measurements were performed with an Agilent QTOF 6520 mass spectrometer, with electron spray ionization (ESI) as the ion source. Specific rotation measurement was performed on Anton Paar MCP500. Flash column chromatography was carried out using a commercially available 200−300 mesh adsorbent under pressure. The purity of the target compounds was determined by high-performance liquid chromatography (HPLC), which was performed on a Shimadzu Labsolutions system with an Agilent C18 column (4.6 × 150 mm, 5 μm). The gradient mobile phase consisted of A (90:10 H_2O/MeCN) and B (5:95 H_2O/MeCN) at a flow rate of 1.5 mL/min. The UV wavelength for detection was 254 nm. The gradient program was as follows: 35−100% B (0−10 min), 100% B (10−12 min), and 35% B (12−15 min). The purity of the target compounds was determined to be higher than 95%.

*2,2′-(2-Methyl-1,3-phenylene)bis(4,4,5,5-tetramethyl-1,3,2-dioxaborolane) (**11**).* 1,3-Dibromo-2-methylbenzene (2 g, 8 mmol) and bis(pinacolato)diborane (4.8 g, 19.2 mmol) were dissolved in dioxane (25 mL). Then, Pd(dppf)Cl_2 (400 mg, 6% mol) and KOAc (4.8 g, 48 mmol) were added. The reaction mixture was degasified with N_2, heated at 130 °C overnight, and detected by TLC. The mixture was filtered, and the solvent was removed under reduced pressure. The resulting crude product was purified on a silica gel column, eluting with EA in PE (1: 20) to obtain **11** (2.26 g) as a white solid, yield 82%. ^{1}H NMR (400 MHz, chloroform-*d*): δ 7.79 (d, J = 7.4 Hz, 2H), 7.14 (t, J = 7.4 Hz, 1H), 2.74 (s, 3H), 1.34 (s, 24H). ESI-MS *m/z*: for $C_{19}H_{31}B_2O_4^+$ $[M + H]^+$ calcd, 345.2; found, 345.2.

*(2-(2-Methyl-3-(4,4,5,5-tetramethyl-1,3,2-dioxaborolan-2-yl)-phenyl)pyridin-4-yl)methanol (**12a**).* (2-Chloropyridin-4-yl)-methanol (100 mg, 0.7 mmol) and **11** (358 mg, 1.04 mmol) were dissolved in the solution of 5 mL dioxane/H_2O (10: 1). Then, tetrakis(triphenylphosphine) palladium (20 mg, 10 % mmol) and K_2CO_3 (276 mg, 2 mmol) were added. The reaction mixture was degasified with N_2, heated at 85 °C for 4 h, and detected by TLC. The mixture was filtered, and the solvent was removed under reduced pressure. The resulting crude product was purified on a silica gel column, eluting with MeOH in DCM (1: 50) to obtain **12a** (180 mg) as a white solid, yield 75%. ^{1}H NMR (400 MHz, chloroform-*d*): δ 8.62 (d, J = 4.6 Hz, 1H), 7.80 (d, J = 7.4 Hz, 1H), 7.29−7.27 (m, 2H), 7.22−7.18 (m, 2H), 4.79 (s, 2H), 2.45 (s, 3H). ESI-MS *m/z*: for $C_{19}H_{25}BNO_3^+$ $[M + H]^+$ calcd, 326.2; found, 326.2.

*(6-(2-Methyl-3-(4,4,5,5-tetramethyl-1,3,2-dioxaborolan-2-yl)-phenyl)pyridin-3-yl)methanol (**12b**).* **12b** was prepared according to the preparation method of **12a**, yield 81%. ^{1}H NMR (300 MHz, chloroform-*d*): δ 8.65 (d, J = 1.3 Hz, 1H), 7.84−7.71 (m, 2H), 7.38 (dd, J = 12.7, 7.8 Hz, 2H), 7.25 (t, J = 7.5 Hz, 1H), 4.76 (s, 2H), 2.47 (s, 3H). ESI-MS *m/z*: for $C_{19}H_{25}BNO_3^+$ $[M + H]^+$ calcd, 326.2; found, 326.2.

*(2-(2-Methyl-[1,1′-biphenyl]-3-yl)pyridin-4-yl)methanol (**13a**).* **12a** (100 mg, 0.3 mmol) and bromobenzene (96 mg, 0.6 mmol) were dissolved in the solution of 3 mL THF/H_2O (3:1). Then, XPhos palladacycle Gen. 2 (XPhos Pd G2, 24 mg, 10 % mmol) and K_3PO_4 (130 mg, 0.61 mmol) were added. The reaction mixture was degasified with N_2, heated at 80 °C overnight, and detected by TLC. The solvent was removed under reduced pressure. The resulting crude product was purified on a silica gel column, eluting with MeOH in DCM (1:50) to obtain **13a** (98 mg) as a white solid, yield 87%. ^{1}H NMR (400 MHz, chloroform-*d*): δ 8.61 (d, J = 5.2 Hz, 1H), 7.44−

https://doi.org/10.1021/acs.jmedchem.1c00010
J. Med. Chem. 2021, 64, 7390−7403

7.35 (m, 4H), 7.29 (dd, J = 6.8, 4.4 Hz, 3H), 7.18 (dd, J = 5.1, 0.7 Hz, 3H), 4.79 (s, 2H), 2.12 (s, 3H). ESI-MS m/z: for $C_{19}H_{18}NO^+$ $[M + H]^+$ calcd, 276.1; found, 276.1.

*(6-(2-Methyl-[1,1′-biphenyl]-3-yl)pyridin-3-yl)methanol (**13b**).* **13b** was prepared according to the preparation method of **13a**, yield 83%. ^{1}H NMR (300 MHz, chloroform-d): δ 8.71−8.64 (m, 1H), 7.80 (dd, J = 8.0, 2.3 Hz, 1H), 7.54−7.26 (m, 9H), 4.79 (s, 2H), 2.16 (s, 3H). ESI-MS m/z: for $C_{19}H_{18}NO^+$ $[M + H]^+$ calcd, 276.1; found, 276.1.

*2-(2-Methyl-[1,1′-biphenyl]-3-yl)isonicotinaldehyde (**14a**).* **13a** (90 mg, 0.33 mmol) and $NaHCO_3$ (55 mg, 0.65 mmol) were dissolved in 5 mL of DCM. To the mixture, DMP (165 mg, 0.39 mmol) was added and stirred at room temperature for 0.5 h. Then, saturated NaS_2O_3 aq was added, and the mixture was diluted with water and extracted with DCM. The combined organic phase was washed with water and saturated NaCl aq and concentrated in vacuo. The crude product was purified on a silica gel column, eluting with EtOAc in PE (1:8) to obtain **14a** as a white solid, yield 84%. ^{1}H NMR (400 MHz, chloroform-d): δ 10.12 (s, 1H), 8.74 (d, J = 4.8 Hz, 1H), 7.61−7.46 (m, 4H), 7.34−7.22 (m, 3H), 7.15 (d, J = 5.2 Hz, 3H), 2.16 (s, 3H). ESI-MS m/z: for $C_{19}H_{16}NO^+$ $[M + H]^+$ calcd, 274.0; found, 274.0.

*6-(2-Methyl-[1,1′-biphenyl]-3-yl)nicotinaldehyde (**14b**).* **14b** was prepared according to the preparation method of **14a**, yield 78%. ^{1}H NMR (400 MHz, chloroform-d): δ 10.18 (s, 1H), 9.17 (dd, J = 2.1, 0.8 Hz, 1H), 8.26 (dd, J = 8.1, 2.2 Hz, 1H), 7.64 (dt, J = 8.0, 0.7 Hz, 1H), 7.46−7.32 (m, 8H), 2.20 (s, 3H). ^{13}C NMR (101 MHz, $CDCl_3$): δ 190.7, 166.0, 151.9, 143.6, 141.9, 140.4, 136.1, 133.5, 131.0, 129.6, 129.4, 128.9, 128.3, 127.1, 125.9, 125.0, 18.6. ESI-MS m/z: for $C_{19}H_{16}NO^+$ $[M + H]^+$ calcd, 274.0; found, 274.0.

*2-(((2-(2-Methyl-[1,1′-biphenyl]-3-yl)pyridin-4-yl)methyl)amino)-ethan-1-ol (**15**).* Compound **14a** (60 mg, 0.2 mmol) was dissolved in DCM (1.5 mL) and MeOH (1.5 mL). 2-aminoethan-1-ol (15 mg, 0.24 mmol) and acetic acid (0.02 mL) were added, and the reaction mixture was stirred at rt for 1 h. $NaCNBH_3$ (62 mg, 1 mmol) was added, and the mixture was stirred at rt overnight and detected by TLC. The solvent was removed under reduced pressure, and the crude product was purified on a silica gel column, eluting with MeOH in DCM (1: 10) to obtain **15** as a white solid, yield 78%. ^{1}H NMR (500 MHz, chloroform-d): δ 8.64 (d, J = 5.1 Hz, 1H), 7.41 (d, J = 7.2 Hz, 3H), 7.37−7.33 (m, 4H), 7.31 (t, J = 7.4 Hz, 1H), 7.28−7.26 (m, 1H), 7.26−7.23 (m, 1H), 3.91 (s, 2H), 3.70 (t, J = 5.1 Hz, 2H), 2.85 (t, J = 5.1 Hz, 2H), 2.15 (s, 3H). ^{13}C NMR (126 MHz, $CDCl_3$): δ 161.0, 149.4, 149.0, 143.3, 142.3, 141.5, 133.4, 130.1, 129.5, 128.9, 128.2, 127.0, 125.6, 123.7, 121.2, 61.0, 52.4, 50.7, 18.5. HRMS (ESI): for $C_{21}H_{23}N_2O^+$ $[M + H]^+$ calcd, 319.1805; found, 319.1809. HPLC, t_R = 4.918 min, purity 98.2%.

*2-(((6-(2-Methyl-[1,1′-biphenyl]-3-yl)pyridin-3-yl)methyl)amino)-ethan-1-ol (**16**).* Compound **14b** (60 mg, 0.2 mmol) was dissolved in DCM (1.5 mL) and MeOH (1.5 mL). 2-aminoethan-1-ol (15 mg, 0.24 mmol) and acetic acid (0.02 mL) were added, and the reaction mixture was stirred at rt for 1 h. $NaCNBH_3$ (62 mg, 1 mmol) was added, and the reaction mixture was stirred at rt overnight and detected by TLC. The solvent was removed under reduced pressure, and the crude product was purified on a silica gel column, eluting with MeOH in DCM (1:10) to obtain **16** as a white solid, yield 73%. ^{1}H NMR (400 MHz, chloroform-d): δ 8.63 (d, J = 2.2 Hz, 1H), 7.76 (dd, J = 8.0, 2.3 Hz, 1H), 7.46−7.26 (m, 9H), 3.87 (s, 2H), 3.69 (t, J = 5.1 Hz, 2H), 2.84 (t, J = 5.1 Hz, 2H), 2.15 (s, 3H). ^{13}C NMR (75 MHz, $CDCl_3$): δ 159.5, 149.0, 143.2, 142.3, 141.2, 136.3, 133.4, 133.3, 130.1, 129.5, 128.9, 128.2, 126.9, 125.6, 124.3, 61.0, 50.9, 50.8, 18.5. HRMS (ESI): for $C_{21}H_{23}N_2O^+$ $[M + H]^+$ calcd, 319.1805; found, 319.1810. HPLC, t_R = 4.079 min, purity 98.9%.

*N-(2-(((6-(2-Methyl-[1,1′-biphenyl]-3-yl)pyridin-3-yl)methyl)-amino)ethyl)acetamide (**17**).* Compound **14b** (60 mg, 0.2 mmol) was dissolved in DCM (1.5 mL) and MeOH (1.5 mL). *N*-(2-aminoethyl)acetamide (24 mg, 0.24 mmol) and acetic acid (0.02 mL) were added, and the reaction mixture was stirred at rt for 1 h. $NaCNBH_3$ (62 mg, 1 mmol) was added, and the mixture was stirred at rt overnight and detected by TLC. The solvent was removed under reduced pressure, and the crude product was purified on a silica gel column, eluting with MeOH in DCM (1:10) to obtain **17** as a white solid, yield 79%. ^{1}H NMR (300 MHz, chloroform-d): δ 8.71−8.56 (m, 1H), 7.73 (dd, J = 8.0, 2.3 Hz, 1H), 7.51−7.26 (m, 9H), 3.85 (s, 2H), 3.38 (q, J = 5.7 Hz, 2H), 2.82 (t, J = 5.8 Hz, 2H), 2.15 (s, 3H), 1.97 (s, 3H). ^{13}C NMR (75 MHz, $CDCl_3$): δ 170.6, 159.6, 149.0, 143.2, 142.3, 141.2, 136.2, 133.4, 133.3, 130.1, 129.4, 128.9, 128.2, 126.9, 125.6, 124.2, 50.8, 48.4, 39.2, 23.4, 18.4. HRMS (ESI): for $C_{23}H_{26}N_3O^+$ $[M + H]^+$ calcd, 360.2070; found, 360.2072. HPLC, t_R = 5.431 min, purity 97.4%.

*Methyl 6-Chloro-2-methoxynicotinate (**19**).* MeOH (830 mg, 26 mmol) was dissolved in 15 mL of THF, and the reaction mixture was stirred at 0 °C. NaH was added, and the reaction mixture was stirred for 0.5 h. Then, **18** (1 g, 5.2 mmol) was added to the reaction mixture and stirred at 60 °C for 2 h. The mixture was cooled to 0 °C and filtered. The filter cake was dissolved in 20 mL of MeOH, and the mixture was stirred at 0 °C. $SOCl_2$ (1.9 g, 16 mmol) was added and stirred for 3 h at reflux. Then, the mixture was cooled, concentrated in vacuo, diluted with water, and extracted with DCM. The combined organic phase was washed with water and saturated NaCl aq and concentrated in vacuo. The crude product was purified on a silica gel column, eluting with EtOAc in PE (1:50) to obtain **19** as a white solid, yield 91%. ^{1}H NMR (400 MHz, chloroform-d): δ 8.13 (d, J = 7.9 Hz, 1H), 6.96 (d, J = 7.9 Hz, 1H), 4.05 (s, 3H), 3.89 (s, 3H). ESI-MS m/z: for $C_8H_8ClNaNO_3^+$ $[M + Na]^+$ calcd, 224.0; found, 224.0.

*Methyl 2-Methoxy-6-(2-methyl-3-(4,4,5,5-tetramethyl-1,3,2-dioxaborolan-2-yl)-phenyl)nicotinate (**20**).* **19** (10 g, 50 mmol) and **11** (21.3 g, 62 mmol) were dissolved in 150 mL of 1,4-dioxane/H_2O (10:1). Tetrakis(triphenylphosphine) palladium (5.8 g, 10% mmol) and K_2CO_3 (17.5 g, 124 mmol) were added to the mixture, which was was degasified with N_2 and heated at 85 °C for 4 h and detected by TLC. The reaction mixture was filtered, and the solvent was removed under reduced pressure. The resulting crude product was purified on a silica gel column, eluting with EtOAc in PE (1:30) to obtain **20** as a white solid, yield 65%. ^{1}H NMR (300 MHz, chloroform-d): δ 8.22 (d, J = 7.7 Hz, 1H), 7.82 (dd, J = 7.4, 1.6 Hz, 1H), 7.45 (dd, J = 7.6, 1.6 Hz, 1H), 7.26 (t, J = 7.5 Hz, 1H), 7.03 (d, J = 7.7 Hz, 1H), 4.05 (s, 3H), 3.92 (s, 3H), 2.56 (s, 3H), 1.36 (s, 12H). ESI-MS m/z: for $C_{21}H_{26}BNaNO_5^+$ $[M + Na]^+$ calcd, 406.2; found, 406.2.

*(2-Methoxy-6-(2-methyl-3-(4,4,5,5-tetramethyl-1,3,2-dioxaborolan-2-yl)phenyl)-pyridin-3-yl)MeOH (**21**).* $LiAlH_4$ (2.1 g, 55 mmol) was slowly added to 50 mL of THF, and the mixture was stirred at 0 °C. **20** (7 g, 18 mmol) was added to the mixture, and the reaction mixture was stirred at rt for 3 h. Then, the mixture was concentrated in vacuo, diluted with water, and extracted with DCM. The combined organic phase was washed with water and saturated NaCl aq. and concentrated *in vacuo* to obtain **21** as a white solid, yield 71%. ^{1}H NMR (400 MHz, chloroform-d): δ 7.81 (dd, J = 7.4, 1.6 Hz, 1H), 7.62 (dd, J = 7.4, 1.0 Hz, 1H), 7.45 (dd, J = 7.6, 1.6 Hz, 1H), 7.31−7.23 (m, 2H), 6.96 (dd, J = 7.3, 1.1 Hz, 1H), 4.70 (d, J = 6.0 Hz, 2H), 4.01 (d, J = 1.1 Hz, 3H), 2.57 (s, 3H), 1.38 (d, J = 1.1 Hz, 12H). ESI-MS m/z: for $C_{20}H_{26}BNaNO_4^+$ $[M + Na]^+$ calcd, 378.2; found, 378.2.

*(2-Methoxy-6-(2-methyl-[1,1′-biphenyl]-3-yl)pyridin-3-yl)MeOH (**22a**).* **22a** was prepared from **21** and bromobenzene according to the preparation method of **13a**, yield 79%. ^{1}H NMR (400 MHz, MeOH-d_4): δ 7.80−7.75 (m, 1H), 7.40 (dd, J = 8.0, 6.6 Hz, 2H), 7.34−7.24 (m, 5H), 7.19 (dd, J = 7.6, 1.6 Hz, 1H), 7.04 (d, J = 7.4 Hz, 1H), 4.64 (s, 2H), 3.94 (s, 3H), 2.16 (s, 3H). ^{13}C NMR (101 MHz, $CDCl_3$): δ 160.7, 157.2, 143.3, 142.4, 141.0, 137.0, 133.8, 130.0, 129.5, 129.0, 128.2, 126.9, 125.5, 121.2, 117.4, 61.1, 53.6, 18.7. ESI-MS m/z: for $C_{20}H_{20}NO_2^+$ $[M + H]^+$ calcd, 306.1; found, 306.1.

*(2-Methoxy-6-(3′-methoxy-2-methyl-[1,1′-biphenyl]-3-yl)-pyridin-3-yl)MeOH (**22b**).* **22b** was prepared from **21** and 1-bromo-3-methoxybenzene according to the preparation method of **13a**, yield 88%. ^{1}H NMR (300 MHz, chloroform-d): δ 7.64 (d, J = 7.3 Hz, 1H), 7.45−7.27 (m, 4H), 7.03 (d, J = 7.3 Hz, 1H), 7.00−6.84 (m, 3H), 4.70 (s, 2H), 4.02 (s, 3H), 3.84 (s, 3H), 2.25 (s, 3H). ^{13}C NMR (75 MHz, $CDCl_3$): δ 160.8, 159.7, 157.4, 144.0, 143.3, 141.3, 137.0, 133.8, 129.9, 129.2, 129.1, 125.5, 122.1, 121.4, 117.4, 115.4, 112.7,

https://doi.org/10.1021/acs.jmedchem.1c00010
J. Med. Chem. 2021, 64, 7390−7403

61.0, 55.4, 53.6, 18.5. ESI-MS *m/z*: for $C_{21}H_{22}NO_3^+$ $[M + H]^+$ calcd, 336.2; found, 336.2.

*(6-(3-(Benzo[d][1,3]dioxol-5-yl)-2-methylphenyl)-2-methoxypyridin-3-yl)MeOH (**22c**).* **22c** was prepared from **21** and 5-bromobenzo-[*d*][1,3]dioxole according to the preparation method of **13a**, yield 72%. ^{1}H NMR (300 MHz, chloroform-*d*): δ 7.66 (d, J = 7.4 Hz, 1H), 7.41 (dd, J = 7.2, 2.0 Hz, 1H), 7.35−7.27 (m, 2H), 7.05 (d, J = 7.3 Hz, 1H), 6.91−6.80 (m, 3H), 6.03 (s, 2H), 4.73 (s, 2H), 4.04 (s, 3H), 2.27 (s, 3H). ^{13}C NMR (101 MHz, $CDCl_3$): δ 160.8, 157.2, 147.4, 146.6, 142.9, 141.1, 137.1, 136.3, 134.0, 130.1, 128.9, 125.5, 122.8, 121.2, 117.4, 110.2, 108.2, 101.1, 61.2, 53.6, 18.8. ESI-MS *m/z*: for $C_{21}H_{22}NO_3^+$ $[M + H]^+$ calcd, 350.1; found, 350.1.

*(6-(3-(2,3-Dihydrobenzo[b][1,4]dioxin-6-yl)-2-methylphenyl)-2-methoxypyridin-3-yl)MeOH (**22d**).* **22d** was prepared from **21** and 6-bromo-2,3-dihydrobenzo[*b*][1,4]dioxine according to the preparation method of **13a**, yield 83%. ^{1}H NMR (500 MHz, chloroform-*d*): δ 7.64 (d, J = 7.3 Hz, 1H), 7.37 (dd, J = 7.3, 1.8 Hz, 1H), 7.32−7.23 (m, 2H), 7.03 (d, J = 7.4 Hz, 1H), 6.94−6.87 (m, 2H), 6.84 (dd, J = 8.2, 2.0 Hz, 1H), 4.71 (s, 2H), 4.31 (s, 4H), 4.02 (s, 3H), 2.26 (s, 3H). ^{13}C NMR (126 MHz, $CDCl_3$): δ 160.8, 157.4, 143.2, 142.8, 142.7, 141.1, 137.1, 135.9, 134.0, 130.1, 128.9, 125.5, 122.8, 121.2, 118.4, 117.4, 117.0, 64.6, 64.6, 61.3, 53.6, 18.8. ESI-MS *m/z*: for $C_{22}H_{22}NO_4^+$ $[M + H]^+$ calcd, 364.1; found, 364.1.

*2-Methoxy-6-(2-methyl-[1,1′-biphenyl]-3-yl)nicotinaldehyde (**23a**).* **23a** was prepared from **22a** according to the preparation method of **14a**, yield 84%. ^{1}H NMR (400 MHz, chloroform-*d*): δ 10.45 (d, J = 0.8 Hz, 1H), 8.23 (d, J = 7.7 Hz, 1H), 7.49−7.35 (m, 8H), 7.22 (dd, J = 7.7, 0.8 Hz, 1H), 4.14 (s, 3H), 2.31 (s, 3H). ^{13}C NMR (101 MHz, $CDCl_3$): δ 189.2, 164.3, 163.8, 143.6, 142.0, 140.3, 138.0, 133.8, 130.9, 129.5, 128.9, 128.3, 127.1, 125.7, 118.1, 116.9, 54.1, 18.8. ESI-MS *m/z*: for $C_{20}H_{18}NO_2^+$ $[M + H]^+$ calcd, 304.1; found, 304.1.

*2-Methoxy-6-(3′-methoxy-2-methyl-[1,1′-biphenyl]-3-yl)-nicotinaldehyde (**23b**).* **23b** was prepared from **22b** according to the preparation method of **14a**, yield 79%. ^{1}H NMR (300 MHz, chloroform-*d*): δ 10.41 (s, 1H), 8.19 (d, J = 7.7 Hz, 1H), 7.49−7.27 (m, 5H), 7.18 (d, J = 7.7 Hz, 1H), 6.99−6.86 (m, 3H), 4.11 (s, 3H), 3.85 (s, 3H), 2.28 (s, 3H). ^{13}C NMR (75 MHz, $CDCl_3$): δ 188.9, 164.4, 163.9, 159.8, 143.7, 142.4, 140.5, 138.1, 133.9, 130.7, 129.3, 129.0, 129.0, 125.7, 122.1, 118.1, 115.5, 112.8, 55.5, 54.1, 18.6. ESI-MS *m/z*: for $C_{21}H_{20}NO_3^+$ $[M + H]^+$ calcd, 334.1; found, 334.1.

*6-(3-(Benzo[d][1,3]dioxol-5-yl)-2-methylphenyl)-2-methoxynicotinaldehyde (**23c**).* **23c** was prepared from **22c** according to the preparation method of **14a**, yield 68%. ^{1}H NMR (500 MHz, chloroform-*d*): δ 10.41 (s, 1H), 7.72 (t, J = 7.4 Hz, 1H), 7.42 (d, J = 7.1 Hz, 1H), 7.31 (q, J = 8.3, 7.8 Hz, 2H), 7.17 (d, J = 7.7 Hz, 1H), 6.92−6.76 (m, 3H), 6.01 (s, 2H), 4.10 (s, 3H), 2.27 (s, 3H). ^{13}C NMR (126 MHz, $CDCl_3$): δ 189.2, 164.3, 163.8, 147.5, 146.8, 143.3, 140.4, 138.1, 134.0, 131.0, 128.8, 125.7, 122.8, 118.1, 117.0, 110.1, 108.3, 101.2, 54.1, 18.7. ESI-MS *m/z*: for $C_{21}H_{18}NO_4^+$ $[M + H]^+$ calcd, 348.1; found, 348.1.

*6-(3-(2,3-Dihydrobenzo[b][1,4]dioxin-6-yl)-2-methylphenyl)-2-methoxynicotin-aldehyde (**23d**).* **23d** was prepared from **22d** according to the preparation method of **14a**, yield 88%. ^{1}H NMR (400 MHz, chloroform-*d*): δ 10.41 (d, J = 0.7 Hz, 1H), 8.19 (d, J = 7.7 Hz, 1H), 7.41 (dd, J = 6.2, 3.0 Hz, 1H), 7.34−7.29 (m, 2H), 7.17 (dd, J = 7.6, 0.7 Hz, 1H), 6.92 (d, J = 8.3 Hz, 1H), 6.89 (d, J = 2.0 Hz, 1H), 6.83 (dd, J = 8.2, 2.1 Hz, 1H), 4.31 (s, 4H), 4.11 (s, 3H), 2.29 (s, 3H). ^{13}C NMR (101 MHz, $CDCl_3$): δ 189.2, 164.3, 163.7, 143.2, 143.0, 142.8, 140.3, 138.0, 135.4, 133.9, 130.9, 128.7, 125.7, 122.7, 118.3, 118.0, 117.0, 116.9, 64.55, 64.5, 54.1, 18.9. ESI-MS *m/z*: for $C_{22}H_{19}NaNO_4^+$ $[M + Na]^+$ calcd, 384.1; found, 384.1.

*2-(((2-Methoxy-6-(2-methyl-[1,1′-biphenyl]-3-yl)pyridin-3-yl)-methyl)amino)ethan-1-ol (**24**).* **24** was prepared from **23a** and 2-aminoethan-1-ol according to the preparation method of **15**, yield 71%. ^{1}H NMR (300 MHz, chloroform-*d*): δ 7.59 (d, J = 7.4 Hz, 1H), 7.46−7.28 (m, 8H), 7.01 (d, J = 7.3 Hz, 1H), 4.00 (s, 3H), 3.82 (s, 2H), 3.73−3.66 (m, 2H), 2.87−2.80 (m, 2H), 2.25 (s, 3H). ^{13}C NMR (101 MHz, $CDCl_3$): δ 161.2, 156.8, 143.3, 142.4, 141.1, 138.1, 133.8, 130.0, 129.5, 129.0, 128.2, 126.9, 125.5, 120.1, 117.2, 60.9, 53.6, 50.5, 48.2, 18.8. HRMS (ESI): for $C_{22}H_{25}N_2O_2^+$ $[M + H]^+$, 349.1911; found, 349.1912. HPLC, t_R = 5.012 min, purity 98.3%.

*N-(2-(((2-Methoxy-6-(2-methyl-[1,1′-biphenyl]-3-yl)pyridin-3-yl)-methyl)amino)-ethyl)acetamide (**25**).* **25** was prepared from **23a** and *N*-(2-aminoethyl)acetamide according to the preparation method of **15**, yield 83%. $[\alpha]_D^{20.0}$ −34.213 (c = 0.5, H_2O). ^{1}H NMR (300 MHz, chloroform-*d*): δ 7.57 (d, J = 7.4 Hz, 1H), 7.45−7.28 (m, 8H), 7.02 (d, J = 7.2 Hz, 1H), 4.00 (s, 3H), 3.80 (s, 2H), 3.40 (q, J = 5.6 Hz, 2H), 2.81 (dd, J = 7.0, 4.5 Hz, 2H), 2.25 (s, 3H), 2.00 (s, 3H). ^{13}C NMR (126 MHz, MeOD): δ 173.6, 162.5, 158.5, 144.6, 143.7, 142.4, 139.9, 134.5, 130.7, 130.4, 129.8, 129.2, 127.9, 126.4, 120.7, 118.3, 54.1, 49.1, 48.6, 39.9, 22.6, 18.8. HRMS (ESI): for $C_{24}H_{28}N_3O_2^+$ $[M + H]^+$, 390.2176; found, 390.2178. HPLC, t_R = 5.506 min, purity 98.7%.

*((2-Methoxy-6-(2-methyl-[1,1′-biphenyl]-3-yl)pyridin-3-yl)-methyl)-L-serine (**26**).* **26** was prepared from **23a** and L-serine according to the preparation method of **15**, yield 39%. ^{1}H NMR (400 MHz, DMSO-d_6): δ 7.87 (d, J = 7.5 Hz, 1H), 7.46 (t, J = 7.3 Hz, 2H), 7.41−7.30 (m, 5H), 7.25 (dd, J = 7.5, 1.7 Hz, 1H), 7.16 (d, J = 7.4 Hz, 1H), 3.91 (s, 5H), 3.75−3.67 (m, 3H), 2.17 (s, 3H). ^{13}C NMR (126 MHz, DMSO): δ 170.9, 160.4, 156.7, 142.6, 141.6, 140.6, 139.5, 132.9, 129.7, 129.2, 128.8, 128.3, 127.1, 125.6, 117.2, 116.2, 63.3, 60.9, 53.5, 44.9, 18.4. HRMS (ESI): for $C_{23}H_{25}N_2O_4^+$ $[M + H]^+$, 393.1809; found, 393.1815. HPLC, t_R = 3.880 min, purity 95.7%.

*(S)-5-((((2-Methoxy-6-(2-methyl-[1,1′-biphenyl]-3-yl)pyridin-3-yl)methyl)amino)-methyl)pyrrolidin-2-one (**27**).* **27** was prepared from **23a** and (*S*)-5-(aminomethyl)pyrrolidin-2-one according to the preparation method of **15**, yield 64%. $[\alpha]_D^{20.0}$ 20.946 (c = 0.5, EtOH). ^{1}H NMR (500 MHz, MeOH-d_4): δ 7.70 (d, J = 7.5 Hz, 1H), 7.40 (t, J = 7.5 Hz, 2H), 7.36−7.27 (m, 5H), 7.21 (dd, J = 7.4, 1.5 Hz, 1H), 7.04 (d, J = 7.4 Hz, 1H), 3.97 (s, 3H), 3.83−3.78 (m, 3H), 2.68 (qd, J = 12.1, 6.2 Hz, 2H), 2.32 (dd, J = 12.4, 7.0 Hz, 2H), 2.28−2.22 (m, 1H), 2.17 (s, 3H), 1.84−1.75 (m, 1H). ^{13}C NMR (126 MHz, MeOD): δ 180.9, 162.4, 158.3, 144.5, 143.7, 142.4, 139.7, 134.5, 130.7, 130.4, 129.8, 129.2, 128.0, 126.4, 120.9, 118.3, 55.7, 55.3, 54.1, 54.0, 31.0, 25.9, 18.8. HRMS (ESI): for $C_{25}H_{28}N_3O_2^+$ $[M + H]^+$, 402.2176; found, 402.2180. HPLC, t_R = 5.067 min, purity 97.0%.

*2-(((2-Methoxy-6-(2-methyl-[1,1′-biphenyl]-3-yl)pyridin-3-yl)-methyl) (methyl)amino)-ethan-1-ol (**28**).* **28** was prepared from **23a** and 2-(methylamino)ethan-1-ol according to the preparation method of **15**, yield 60%. ^{1}H NMR (600 MHz, chloroform-*d*): δ 7.61 (d, J = 7.3 Hz, 1H), 7.45−7.41 (m, 3H), 7.40−7.34 (m, 3H), 7.32 (t, J = 7.5 Hz, 1H), 7.28 (dd, J = 7.6, 1.5 Hz, 1H), 7.03 (d, J = 7.4 Hz, 1H), 4.00 (s, 3H), 3.70 (t, J = 5.4 Hz, 2H), 3.60 (s, 2H), 2.69 (t, J = 5.3 Hz, 2H), 2.30 (s, 3H), 2.27 (s, 3H). ^{13}C NMR (151 MHz, $CDCl_3$): δ 161.3, 156.8, 143.3, 142.5, 141.1, 139.0, 133.8, 130.0, 129.5, 129.0, 128.2, 126.9, 125.5, 118.9, 117.1, 59.0, 58.7, 55.6, 53.6, 42.2, 18.8. HRMS (ESI): for $C_{23}H_{28}N_2O_2^+$ $[M + H]^+$, 363.2067; found, 363.2071. HPLC, t_R = 6.184 min, purity 96.3%.

*(R)-2-(((2-Methoxy-6-(2-methyl-[1,1′-biphenyl]-3-yl)pyridin-3-yl)-methyl)amino)-propan-1-ol (**29**).* **29** was prepared from **23a** and (*R*)-2-aminopropan-1-ol according to the preparation method of **15**, yield 82%. $[\alpha]_D^{20.0}$ −27.151 (c = 0.5, EtOH). ^{1}H NMR (600 MHz, chloroform-*d*): δ 7.63 (d, J = 7.4 Hz, 1H), 7.45−7.41 (m, 3H), 7.40−7.35 (m, 3H), 7.32 (t, J = 7.5 Hz, 1H), 7.28 (d, J = 7.5 Hz, 1H), 7.02 (d, J = 7.3 Hz, 1H), 4.01 (s, 3H), 3.90 (d, J = 13.7 Hz, 1H), 3.78 (d, J = 13.6 Hz, 1H), 3.66 (dd, J = 10.7, 3.9 Hz, 1H), 3.36 (dd, J = 10.7, 6.8 Hz, 1H), 2.91−2.86 (m, 1H), 2.26 (s, 3H), 1.13 (d, J = 6.5 Hz, 3H). ^{13}C NMR (151 MHz, $CDCl_3$): δ 161.1, 156.8, 143.3, 142.4, 141.1, 138.1, 133.7, 130.0, 129.5, 129.0, 128.2, 126.9, 125.5, 120.1, 117.3, 65.4, 54.0, 53.6, 45.8, 18.7, 17.2, 17.1. HRMS (ESI): for $C_{23}H_{28}N_2O_2^+$ $[M + H]^+$, 363.2067; found, 363.2072. HPLC, t_R = 7.882 min, purity 97.4%.

*3-(((2-Methoxy-6-(2-methyl-[1,1′-biphenyl]-3-yl)pyridin-3-yl)-methyl)amino)propan-1-ol (**30**).* **30** was prepared from **23a** and 3-aminopropan-1-ol according to the preparation method of **15**, yield 79%. ^{1}H NMR (600 MHz, chloroform-*d*): δ 7.58 (d, J = 7.4 Hz, 1H), 7.42 (q, J = 7.5 Hz, 3H), 7.39−7.33 (m, 3H), 7.31 (t, J = 7.5 Hz, 1H), 7.27 (dd, J = 7.6, 1.6 Hz, 1H), 7.01 (d, J = 7.3 Hz, 1H), 4.00 (s, 3H), 3.86−3.81 (m, 4H), 2.93 (t, J = 5.7 Hz, 2H), 2.25 (s, 3H), 1.77 (dp, J

https://doi.org/10.1021/acs.jmedchem.1c00010
J. Med. Chem. 2021, 64, 7390−7403

= 10.4, 5.5, 5.1 Hz, 2H). ^{13}C NMR (151 MHz, $CDCl_3$): δ 161.2, 157.0, 143.3, 142.4, 141.0, 138.4, 133.8, 130.0, 129.5, 129.0, 128.2, 126.9, 125.5, 119.3, 117.2, 64.2, 53.6, 49.3, 48.6, 30.6, 18.8. HRMS (ESI): for $C_{23}H_{28}N_2O_2^+$ $[M + H]^+$, 363.2067; found, 363.2067. HPLC, t_R = 5.284 min, purity 98.9%.

*(R)-1-((2-Methoxy-6-(2-methyl-[1,1′-biphenyl]-3-yl)pyridin-3-yl)methyl)pyrrolidin-3-ol (**31**).* **31** was prepared from **23a** and (R)-pyrrolidin-3-ol according to the preparation method of **15**, yield 56%. $[\alpha]_D^{20.0}$ −120.752 (*c* = 0.25, EtOH). ^{1}H NMR (300 MHz, chloroform-*d*): δ 7.70 (d, *J* = 7.4 Hz, 1H), 7.39 (tdd, *J* = 10.9, 10.2, 4.8, 2.2 Hz, 6H), 7.32−7.27 (m, 2H), 7.03 (d, *J* = 7.4 Hz, 1H), 4.37 (tt, *J* = 4.7, 2.4 Hz, 1H), 3.98 (s, 3H), 3.70 (s, 2H), 3.00 (td, *J* = 8.6, 4.9 Hz, 1H), 2.81 (dd, *J* = 10.1, 2.1 Hz, 1H), 2.64 (dd, *J* = 10.2, 5.2 Hz, 1H), 2.51−2.37 (m, 2H), 2.30−2.27 (m, 1H), 2.26 (s, 3H), 1.87−1.71 (m, 1H). ^{13}C NMR (151 MHz, $CDCl_3$): δ 161.0, 156.6, 143.3, 142.5, 141.2, 138.7, 133.8, 129.9, 129.5, 129.1, 128.2, 126.9, 125.5, 118.8, 117.2, 71.4, 63.2, 53.6, 53.3, 52.8, 35.1, 18.8. HRMS (ESI): for $C_{24}H_{27}N_2O_2^+$ $[M + H]^+$, 375.2067; found, 375.2072. HPLC, t_R = 6.330 min, purity 97.8%.

*N1-((2-Methoxy-6-(2-methyl-[1,1′-biphenyl]-3-yl)pyridin-3-yl)methyl)ethane-1,2-diamine (**32**).* **32** was prepared from **23a** and *tert*-butyl (2-aminoethyl)carbamate according to the preparation method of **15**, yield 86%. ^{1}H NMR (600 MHz, MeOH-d_4): δ 7.88 (d, *J* = 7.5 Hz, 1H), 7.41 (t, *J* = 7.6 Hz, 2H), 7.37−7.28 (m, 5H), 7.23 (dd, *J* = 7.5, 1.5 Hz, 1H), 7.14 (d, *J* = 7.5 Hz, 1H), 4.31 (s, 2H), 4.04 (s, 3H), 3.41 (dt, *J* = 33.3, 6.6 Hz, 4H), 2.18 (s, 3H). ^{13}C NMR (151 MHz, MeOD): δ 162.5, 161.3, 144.6, 143.5, 142.2, 141.8, 134.5, 131.1, 130.3, 129.8, 129.2, 128.0, 126.5, 118.6, 113.3, 54.5, 47.7, 45.6, 37.0, 18.8. HRMS (ESI): for $C_{22}H_{26}N_3O^+$ $[M + H]^+$, 348.2070; found, 348.2073. HPLC, t_R = 4.639 min, purity: 98.4%.

*2-(((2-Methoxy-6-(3′-methoxy-2-methyl-[1,1′-biphenyl]-3-yl)-pyridin-3-yl)methyl)-amino)ethan-1-ol (**33**).* **33** was prepared from **23b** and 2-aminoethan-1-ol according to the preparation method of **15**, yield 67%. ^{1}H NMR (500 MHz, chloroform-*d*): δ 7.64 (d, *J* = 7.4 Hz, 1H), 7.40 (d, *J* = 6.0 Hz, 1H), 7.36−7.26 (m, 3H), 7.04 (d, *J* = 7.4 Hz, 1H), 6.98−6.88 (m, 3H), 4.01 (s, 3H), 3.91 (s, 2H), 3.84 (s, 3H), 3.74 (t, *J* = 5.1 Hz, 2H), 2.88 (t, *J* = 5.0 Hz, 2H), 2.25 (s, 3H). ^{13}C NMR (126 MHz, $CDCl_3$): δ 161.1, 159.4, 157.7, 143.7, 143.2, 140.8, 139.0, 133.7, 129.9, 129.2, 129.0, 125.5, 122.0, 117.6, 117.4, 115.2, 112.4, 59.9, 55.3, 53.8, 50.2, 47.8, 18.7. HRMS (ESI): for $C_{23}H_{27}N_2O_3^+$ $[M + H]^+$, 379.2016; found, 379.2018. HPLC, t_R = 4.786 min, purity 96.6%.

*2-(((6-(3-(Benzo[d][1,3]dioxol-5-yl)-2-methylphenyl)-2-methoxy-pyridin-3-yl)methyl)amino)ethan-1-ol (**34**).* **34** was prepared from **23c** and 2-aminoethan-1-ol according to the preparation method of **15**, yield 70%. ^{1}H NMR (500 MHz, chloroform-*d*): δ 7.60 (d, *J* = 7.4 Hz, 1H), 7.38 (d, *J* = 7.7 Hz, 1H), 7.30−7.24 (m, 2H), 7.00 (d, *J* = 7.3 Hz, 1H), 6.90−6.77 (m, 3H), 6.00 (s, 2H), 4.00 (s, 3H), 3.85 (s, 2H), 3.71 (t, *J* = 5.2 Hz, 2H), 2.85 (t, *J* = 5.3 Hz, 2H), 2.25 (s, 3H). ^{13}C NMR (126 MHz, $CDCl_3$): δ 161.2, 157.2, 147.4, 146.6, 142.9, 141.1, 138.3, 134.0, 133.8, 130.1, 129.0, 125.5, 122.9, 119.6, 117.3, 110.2, 108.2, 101.2, 60.8, 53.7, 50.4, 48.1, 18.8. HRMS (ESI): for $C_{23}H_{25}N_2O_4^+$ $[M + H]^+$, 393.1809; found, 393.1813. HPLC, t_R = 5.226 min, purity 97.1%.

*2-(((6-(3-(2,3-Dihydrobenzo[b][1,4]dioxin-6-yl)-2-methylphenyl)-2-methoxypyridin-3-yl)methyl)amino)ethan-1-ol (**35**).* **35** was prepared from **23d** and 2-aminoethan-1-ol according to the preparation method of **15**, yield 82%. ^{1}H NMR (500 MHz, MeOH-d_4): δ 7.68 (d, *J* = 7.3 Hz, 1H), 7.30 (d, *J* = 6.7 Hz, 1H), 7.23 (t, *J* = 7.6 Hz, 1H), 7.17 (d, *J* = 5.9 Hz, 1H), 7.02 (d, *J* = 7.4 Hz, 1H), 6.85 (d, *J* = 8.2 Hz, 1H), 6.81−6.70 (m, 2H), 4.25 (s, 4H), 3.97 (s, 3H), 3.82 (s, 2H), 3.69 (t, *J* = 5.5 Hz, 2H), 2.75 (t, *J* = 5.5 Hz, 2H), 2.17 (s, 3H). ^{13}C NMR (126 MHz, MeOD): δ 162.5, 158.6, 144.6, 144.1, 144.0, 142.3, 139.9, 136.8, 134.6, 130.8, 129.6, 126.3, 123.4, 120.5, 119.1, 118.2, 117.8, 65.7, 65.7, 61.4, 54.1, 51.7, 48.9, 18.8. HRMS (ESI): for $C_{24}H_{27}N_2O_4^+$ $[M + H]^+$, 407.1965; found, 407.1964. HPLC, t_R = 5.237 min, purity: 96.5%.

*N-(2-(((6-(3-(2,3-Dihydrobenzo[b][1,4]dioxin-6-yl)-2-methyl-phenyl)-2-methoxy-pyridin-3-yl)methyl)amino)ethyl)acetamide (**36**).* **36** was prepared from **23d** and *N*-(2-aminoethyl)acetamide according to the preparation method of **15**, yield 87%. ^{1}H NMR (500 MHz, MeOH-d_4): δ 7.69 (d, *J* = 7.4 Hz, 1H), 7.31 (d, *J* = 7.6 Hz, 1H), 7.25 (t, *J* = 7.6 Hz, 1H), 7.19 (d, *J* = 6.8 Hz, 1H), 7.04 (d, *J* = 7.4 Hz, 1H), 6.87 (d, *J* = 8.2 Hz, 1H), 6.82−6.73 (m, 2H), 4.27 (s, 4H), 3.99 (s, 3H), 3.81 (s, 2H), 3.35 (t, *J* = 6.3 Hz, 2H), 2.76 (t, *J* = 6.3 Hz, 2H), 2.18 (s, 3H), 1.95 (s, 3H). ^{13}C NMR (126 MHz, MeOD): δ 173.6, 162.5, 158.6, 144.6, 144.2, 144.1, 142.3, 140.0, 136.6, 134.6, 130.8, 129.6, 126.3, 123.4, 120.5, 119.1, 118.3, 117.9, 65.7, 65.7, 54.1, 49.1, 48.6, 39.8, 22.6, 18.8. HRMS (ESI): for $C_{26}H_{30}N_3O_4^+$ $[M + H]^+$, 448.2231; found, 448.2238. HPLC, t_R = 5.921 min, purity: 99.2%.

*((6-(3-(2,3-Dihydrobenzo[b][1,4]dioxin-6-yl)-2-methylphenyl)-2-methoxypyridin-3-yl)methyl)-L-serine (**37**).* **37** was prepared from **23d** and L-serine according to the preparation method of **15**, yield 35%. $[\alpha]_D^{20.0}$ −27.248 (*c* = 0.25, H_2O). ^{1}H NMR (400 MHz, DMSO-d_6): δ 7.90 (d, *J* = 7.5 Hz, 1H), 7.37−7.25 (m, 2H), 7.22−7.17 (m, 1H), 7.13 (d, *J* = 7.5 Hz, 1H), 6.91 (d, *J* = 8.2 Hz, 1H), 6.84−6.75 (m, 2H), 4.26 (s, 4H), 4.05 (t, *J* = 15.8 Hz, 2H), 3.89 (s, 3H), 3.78 (d, *J* = 9.0 Hz, 3H), 2.16 (s, 3H). ^{13}C NMR (101 MHz, DMSO): δ 171.4, 160.8, 157.1, 143.4, 143.0, 142.5, 140.9, 140.0, 135.1, 133.4, 130.1, 129.0, 126.0, 122.7, 122.6, 118.2, 117.6, 117.3, 64.6, 63.7, 61.2, 53.9, 45.3, 18.9. HRMS (ESI): for $C_{25}H_{29}N_2O_6^+$ $[M + H]^+$, 451.1864; found, 451.1863. HPLC, t_R = 3.274 min, purity 95.6%.

*N1-((6-(3-(2,3-Dihydrobenzo[b][1,4]dioxin-6-yl)-2-methylphenyl)-2-methoxypyridin-3-yl)methyl)ethane-1,2-diamine (**38**).* **38** was prepared from **23d** and *tert*-butyl (2-aminoethyl)carbamate according to the preparation method of **15**, yield 77%. ^{1}H NMR (400 MHz, chloroform-*d*): δ 7.62 (d, *J* = 7.2 Hz, 1H), 7.28 (dd, *J* = 6.2, 3.3 Hz, 1H), 7.20 (d, *J* = 3.0 Hz, 2H), 6.97 (d, *J* = 7.3 Hz, 1H), 6.88−6.80 (m, 2H), 6.76 (d, *J* = 8.2 Hz, 1H), 4.25 (s, 4H), 4.12 (s, 2H), 3.92 (s, 3H), 3.42 (d, *J* = 21.5 Hz, 4H), 2.19 (s, 3H). ^{13}C NMR (151 MHz, $CDCl_3$): δ 161.2, 160.3, 143.1, 142.8, 142.7, 140.8, 140.4, 135.6, 133.9, 130.4, 128.8, 125.5, 122.7, 118.3, 117.6, 116.9, 110.5, 64.5, 64.5, 53.8, 46.8, 44.8, 36.4, 18.6. HRMS (ESI): for $C_{24}H_{28}N_3O_3^+$ $[M + H]^+$, 406.2125; found, 406.2128. HPLC, t_R = 4.183 min, purity 99.1%.

*3-(((6-(3-(2,3-Dihydrobenzo[b][1,4]dioxin-6-yl)-2-methylphenyl)-2-methoxypyridin-3-yl)methyl)amino)propan-1-ol (**39**).* **39** was prepared from **23d** and 3-aminopropan-1-ol according to the preparation method of **15**, yield 75%. ^{1}H NMR (300 MHz, chloroform-*d*): δ 7.71 (d, *J* = 7.4 Hz, 1H), 7.37 (dd, *J* = 6.2, 3.2 Hz, 1H), 7.30−7.27 (m, 2H), 7.05 (d, *J* = 7.4 Hz, 1H), 6.96−6.81 (m, 3H), 4.32 (s, 4H), 4.06 (s, 2H), 4.03 (s, 3H), 3.77 (d, *J* = 5.3 Hz, 2H), 3.13 (t, *J* = 5.6 Hz, 2H), 2.26 (s, 3H), 1.89 (t, *J* = 5.4 Hz, 2H). ^{13}C NMR (151 MHz, $CDCl_3$): δ 161.1, 159.0, 143.1, 142.8, 142.7, 140.5, 140.0, 135.6, 133.8, 130.4, 128.8, 125.6, 122.7, 118.3, 117.5, 117.0, 113.7, 64.5, 64.5, 62.0, 53.9, 47.9, 47.4, 28.6, 18.8. HRMS (ESI): for $C_{25}H_{29}N_2O_4^+$ $[M + H]^+$, 421.2122; found, 421.2121. HPLC, t_R = 5.330 min, purity 97.2%.

*Methyl 2-Methoxy-6-(2-methyl-[1,1′-biphenyl]-3-yl)nicotinate (**40**).* **40** was prepared from **21** and bromobenzene according to the preparation method of **13a**, yield 80%. ^{1}H NMR (300 MHz, chloroform-*d*): δ 8.26 (d, *J* = 7.7 Hz, 1H), 7.43 (ddd, *J* = 7.4, 4.6, 1.6 Hz, 3H), 7.39−7.30 (m, 5H), 7.12 (d, *J* = 7.7 Hz, 1H), 4.09 (s, 3H), 3.94 (s, 3H), 2.26 (s, 3H). ^{13}C NMR (126 MHz, $CDCl_3$): δ 165.6, 162.1, 161.6, 143.4, 142.0, 141.6, 140.2, 133.7, 130.6, 129.4, 128.8, 128.1, 127.0, 125.6, 116.9, 111.6, 54.3, 52.3, 18.7. HRMS (ESI): for $C_{21}H_{20}NO_3^+$ $[M + H]^+$, 334.1438; found, 334.1442. HPLC, t_R = 6.392 min, purity 96.4%.

*2-Methoxy-6-(2-methyl-3-(4,4,5,5-tetramethyl-1,3,2-dioxaborolan-2-yl)phenyl)-nicotinic Acid (**41**).* **40** (200 mg, 0.52 mmol) and LiOH (60 mg, 2.6 mmol) were dissolved in 4 mL of THF/MeOH/H_2O (3:2:2), and the mixture was stirred at rt for 1 h. Then, the mixture was diluted with water and extracted with EtOAc. To the mixture, 1 N HCl aq was added, and the combined organic phase was washed with water and saturated NaCl aq and concentrated *in vacuo* to obtain **41** as a white solid, yield 93%. ^{1}H NMR (400 MHz, MeOH-d_4): δ 8.26 (d, *J* = 7.7 Hz, 1H), 7.74 (d, *J* = 7.5 Hz, 1H), 7.41 (d, *J* = 7.7 Hz, 1H), 7.22 (t, *J* = 7.5 Hz, 1H), 7.05 (d, *J* = 7.7 Hz, 1H), 3.99 (s, 3H), 2.51 (s, 3H), 1.34 (s, 12H). ^{13}C NMR (101 MHz, MeOD): δ 168.2, 163.7, 162.8, 143.4, 143.1, 142.6, 141.0, 137.3, 133.2, 125.9,

https://doi.org/10.1021/acs.jmedchem.1c00010
J. Med. Chem. 2021, 64, 7390−7403

118.2, 112.8, 84.9, 54.4, 25.2, 20.2. ESI-MS *m/z*: for $C_{20}H_{20}BNO_5^+$ $[M + H]^+$ calcd, 370.2; found, 370.2.

*N-(2-Hydroxyethyl)-2-methoxy-6-(2-methyl-3-(4,4,5,5-tetramethyl-1,3,2-dioxa-borolan-2-yl)phenyl)nicotinamide (**42**).* **41** (100 mg, 0.27 mmol), 2-aminoethan-1-ol (20 mg, 0.33 mmol), HOBT (54 mg, 0.4 mmol), and EDCI (76 mg, 0.4 mmol) were dissolved in 10 mL of DCM, and the reaction mixture was stirred at rt for 2 h. Then, the solvent was removed under reduced pressure. The resulting crude product was purified on a silica gel column, eluting with MeOH in DCM (1: 40) to obtain **42** as a white solid, yield 55%. ^{1}H NMR (400 MHz, MeOH-d_4): δ 8.42 (d, J = 7.7 Hz, 1H), 7.77 (dd, J = 7.5, 1.5 Hz, 1H), 7.46 (dd, J = 7.6, 1.6 Hz, 1H), 7.27 (d, J = 7.6 Hz, 1H), 7.18 (d, J = 7.7 Hz, 1H), 4.12 (s, 3H), 3.76 (t, J = 5.6 Hz, 2H), 3.59 (t, J = 5.6 Hz, 2H), 2.54 (s, 3H), 1.38 (s, 12H). ^{13}C NMR (101 MHz, $CDCl_3$): δ 165.6, 161.3, 159.7, 142.5, 141.9, 141.8, 139.7, 136.5, 132.3, 125.0, 118.4, 113.3, 83.8, 62.8, 54.4, 43.1, 25.0, 20.0. ESI-MS *m/z*: for $C_{20}H_{20}BNaNO_5^+$ $[M + Na]^+$ calcd, 435.2; found, 435.2.

*N-(2-Hydroxyethyl)-2-methoxy-6-(2-methyl-[1,1′-biphenyl]-3-yl)-nicotinamide (**43**).* **43** was prepared from **42** and bromobenzene according to the preparation method of **13a**, yield 71%. ^{1}H NMR (400 MHz, chloroform-*d*): δ 8.55 (d, J = 7.7 Hz, 1H), 8.43 (t, J = 5.6 Hz, 1H), 7.41 (ddd, J = 6.5, 3.5, 1.6 Hz, 3H), 7.38−7.29 (m, 4H), 7.20 (d, J = 7.8 Hz, 1H), 4.12 (s, 3H), 3.83 (t, J = 5.1 Hz, 2H), 3.66 (q, J = 5.4 Hz, 2H), 2.24 (s, 3H). ^{13}C NMR (126 MHz, $CDCl_3$): δ 165.1, 161.0, 159.7, 143.4, 142.0, 141.8, 140.1, 133.6, 130.5, 129.3, 128.9, 128.1, 126.9, 125.6, 118.3, 113.5, 62.0, 54.3, 42.7, 18.6. HRMS (ESI): for $C_{22}H_{23}N_2O_3^+$ $[M + H]^+$, 363.1703; found, 363.1705. HPLC, t_R = 4.526 min, purity 98.4%.

Molecular Modeling. The X-ray structure of PD-L1 was downloaded from the Protein Data Bank (PDB code: 5J89) into Schrodinger Maestro 11.5. The protein structure was prepared by assigning bond orders, adding hydrogens, and generating het states using Epik. H-bond assignment was optimized using PROPKA, and water with less than three H bonds and co-crystallized ligand was removed. Energy minimization with the root-mean-square deviation value of 0.3 was applied using OPLS3 force field. Compound **24** was prepared using the OPLS3 force field, and chiralities were determined from the 3D structure. The docking procedure was performed by employing the DOCK program using Glide 5.8, and the structural image was obtained using PyMOL software.

PD-1/PD-L1 TR-FRET Assay. The PD-1/PD-L1 TR-FRET assay was used to measure the inhibition of PD-1 binding to PD-L1 of the synthesized compounds. The PD-1/PD-L1 binding assay kits (catalog #71105 &79311) were purchased from BPS Bioscience. The experiments were performed according to the instructions of the manufacturer. In brief, 5 μL of PD-L1-biotin (11 μg/mL) and 5 μL of prediluted solution with compounds at the indicated concentration were added and incubated for 15 min at rt. Subsequently, 5 μL of PD-1-Eu (0.2 μg/mL) and 5 μL of dye-labeled acceptor were added to reach a total 20 μL volume for the experimental system, which was then incubated for 90 min at rt. Time-resolved fluorescence intensities were measured using a Molecular Devices instrument (Perkin Elmer EnVision). Tb donor emission was measured at 620 nm, followed by the dye acceptor emission at 665 nm. Data analysis was performed using the TR-FRET ratio (665 nm emission/620 nm emission), and inhibition rate % = (Ratio_max-Ratio_sample)/(Ratio_max-Ratio_min) × 100, where Ratio_max, Ratio_min, and Ratio_sample represented the ratios of the positive control, negative control, and test compounds, respectively. The IC_{50} values were determined using GraphPad Prism 6 software.

PBMC Killing Assay. Fresh PBMCs were isolated from three healthy donors. MDA-MB 231 cells (2×10^3 cells/well) were seeded in 96-well plates 12 h ahead. Different concentrations of compound **24**, compound **1** (500 nM), and durvalumab (5 μg/mL; Selleck, #A2013) were added 2 h ahead. PBMCs (2×10^4 cells/well) were stimulated with the CD3/CD28/CD2 T cell activator (25 μL/mL, ImmunoCult, catalog #10970) for 24 h. The stimulated PBMCs were added to the MDA-MB-231 cells and the test compound and then co-cultured at 37 °C for 12 h. Cell death was evaluated by the quantification of cell damage, which was evaluated by the release of LDH. The level of LDH released to the supernatant was detected by an LDH cytotoxicity assay detection kit (Beyotime, China), following the manufacturer's instructions. MDA-MB-231 cell viability was measured as

$$\text{viability (\%)} = \left(1 - \frac{LD_{231+PBMC+24} - LD_{PBMC+24} - LD_{231+24}}{LD_{231}}\right) \times 100$$

where $LD_{231+PBMC+24}$, $LD_{PBMC+24}$, and LD_{231+24} represented the detected LDH absorbency values of MDA-MB-231 cells treated with PBMCs and different concentrations of compound **24**, PBMCs treated with 1.5 μM compound **24**, and MDA-MB-231 cells treated with 1.5 μM compound **24**. LD_{231} represented the detected LDH absorbency value of MDA-MB-231 cells without PBMCs or compound **24** treated but with full lysis at the end of culture by the lysis buffer.

PK Study in Male SD Rats. The experimental procedures and animal use and care protocols were approved by the Institutional Animal Care and Use Committee (IACUC) of China Pharmaceutical University, following the guidelines of the Association for Assessment and Accreditation of Laboratory Animal Care. Male SD rats (n = 4, 240−260 g) were purchased from Veterinary College of Yangzhou University (Yangzhou, Jiangsu, China). Diet was prohibited for 12 h before the experiment, but water was freely available. Compound **24** was dissolved in 10% ethanol, 40% PEG-300, and 50% DI water for iv administration and intragastric gavage. Blood samples (0.35 mL) were collected from the orbit into heparinized polythene tubes at 0.033, 0.167, 0.5, 1, 2, 3, 5, 8, 12, 16, and 24 h after oral (25 mg/kg) or iv (3 mg/kg) administration of compound **24**. Blood samples were immediately centrifuged at 8000g for 10 min at 4 °C to obtain plasma. The obtained plasma was stored at −20 °C prior to analysis. The plasma concentrations of compound **24** were analyzed by LC−MS/MS. Phoenix WinNonlin was used to calculate all PK parameters.

***In Vivo* Antitumor Activity Study.** The experimental procedures and animal use and care protocols were approved by the Institutional Animal Care and Use Committee (IACUC) of China Pharmaceutical University, following the guidelines of the Association for Assessment and Accreditation of Laboratory Animal Care. Male BALB/c mice between 5 and 6 weeks in age were purchased from Veterinary College of Yangzhou University (Yangzhou, Jiangsu, China). A total of 5×10^5 CT26 cells were inoculated into the right flank of each mouse. The vehicle formulation for compound **24** was 10% ethanol, 40% PEG-300, and 50% DI water and was formulated in a single batch for the entire study. Mice in control groups were treated with 200 μL of vehicle solution only. Mice were treated with vehicle control and compound **24** (40, 80 mg/kg) by intragastric gavage once a day for 2 weeks. The tumor volume sizes were measured every 2 days with a caliper and calculated with the formula 0.5 × length × width. The mice were sacrificed after the treatment, and tumors were excised and weighed.

Flow Cytometry Analysis. Mice were sacrificed and tumors were harvested. 0.3 mg tumor tissue was isolated and added into a solution of collagenase (400 units/mL), DNase 1 (100 μg/mL), and hyaluronidase (0.04 units/mL). The mixture was shaken at 37 °C for 1 h. Then, the mixture was passed through a 70 μm nylon cell strainer. The sample was washed three times with PBS (with 2% FBS) and then resuspended in 1×10^6 cells/mL for flow cytometry analysis. Antibody (AF488 antimouse CD45, PE/Cy7 antimouse CD3, APC antimouse CD4, BV510 antimouse CD8, and PE antimouse FOXP3, all purchased from BioLegend) was added, following the antibody manufacturer's recommendations, and incubated for 30 min on ice. Cells were analyzed on a BD FACS Celesta flow cytometer, and data were analyzed using FlowJo 10. Cellular events were first gated by forward and then by side scattering characteristics. The cell counts for $CD45^+$, $CD45^+CD3^+$, $CD45^+CD3^+CD4^+$, and $CD45^+CD3^+CD4^+FOXP3^+$ $CD45^+CD3^+$-$CD8^+$ were assessed. For

https://doi.org/10.1021/acs.jmedchem.1c00010
J. Med. Chem. 2021, 64, 7390−7403

quantification, the proportion of each immune subpopulation was determined by flow cytometry.

Immunohistochemistry Staining. Isolated tumors were fixed in 4% paraformaldehyde for 24 h at rt, dehydrated, and embedded in paraffin wax. Before staining with antibody, the tissues were transferred to slides and deparaffinized. The antimouse CD8 antibody was added on the slides and incubated at 4 °C overnight for immunofluorescence staining. After washing with PBS three times, tissues were incubated with DAPI. Immunofluorescence images were acquired on a fluorescent inverted microscope (Nikon Eclipse Ts2R).

H&E Staining. The tumor sample was immersed in 4% paraformaldehyde for 4 h and transferred to 70% ethanol. Individual lobes of the tumor sample were placed in processing cassettes, dehydrated through a serial alcohol gradient, and embedded in paraffin wax blocks. 5 μm thick tissue sections were dewaxed in xylene, rehydrated through decreasing concentrations of ethanol, washed in PBS, and stained with H&E. After staining, the sections were dehydrated through increasing concentrations of ethanol and xylene. Images were acquired on a fluorescent inverted microscope (Nikon Eclipse Ts2R).

■ ASSOCIATED CONTENT

Supporting Information

The Supporting Information is available free of charge at https://pubs.acs.org/doi/10.1021/acs.jmedchem.1c00010.

Data of PD-1/PD-L1 TR-FRET assay, *in vivo* antitumor activity study of compound **24**, compound **1** and PD-L1 antibody, binding affinity of compound **1** and **24** to PD-L1 by microscale thermophoresis assay, and ^{1}H NMR, ^{13}C NMR, and HPLC spectra of the final compounds (PDF)

Docking of compound **24** with PD-L1 from 5J89 (CSV)

Molecular formula strings (PDB)

■ AUTHOR INFORMATION

Corresponding Author

Sheng Jiang − *State Key Laboratory of Natural Medicines and Department of Medicinal Chemistry, School of Pharmacy, China Pharmaceutical University, Nanjing 210009, China;* orcid.org/0000-0002-4550-5024; Email: jiangsh9@gmail.com

Authors

Tianyu Wang − *State Key Laboratory of Natural Medicines and Department of Medicinal Chemistry, School of Pharmacy, China Pharmaceutical University, Nanjing 210009, China*

Shi Cai − *State Key Laboratory of Natural Medicines and Department of Medicinal Chemistry, School of Pharmacy, China Pharmaceutical University, Nanjing 210009, China*

Mingming Wang − *State Key Laboratory of Natural Medicines and Department of Medicinal Chemistry, School of Pharmacy, China Pharmaceutical University, Nanjing 210009, China*

Wanheng Zhang − *State Key Laboratory of Natural Medicines and Department of Medicinal Chemistry, School of Pharmacy, China Pharmaceutical University, Nanjing 210009, China*

Kuojun Zhang − *State Key Laboratory of Natural Medicines and Department of Medicinal Chemistry, School of Pharmacy, China Pharmaceutical University, Nanjing 210009, China*

Dong Chen − *State Key Laboratory of Natural Medicines and Department of Medicinal Chemistry, School of Pharmacy, China Pharmaceutical University, Nanjing 210009, China*

Zheng Li − *Center for Bioenergetics, Houston Methodist Research Institute, Houston, Texas 77030, United States;* orcid.org/0000-0001-6118-9175

Complete contact information is available at: https://pubs.acs.org/10.1021/acs.jmedchem.1c00010

Notes

The authors declare no competing financial interest.

■ ACKNOWLEDGMENTS

This work was supported by the National Natural Science Foundation of China (81773559, 21807114, and 82161138005), the Double First-Class University Project (CPU2018GY03).

■ ABBREVIATIONS USED

Ala, alanine; Asp, aspartic acid; AUC, area under the curve; Cl, plasma clearance; C_{max}, maximum plasma concentration; ESI, electron spray ionization; FDA, the US Food and Drug Administration; Gln, glutamine; H&E, hematoxylin and eosin; HPLC, high-performance liquid chromatography; HRMS, high-resolution mass; LDH, lactate dehydrogenase; mAbs, monoclonal antibodies; Met, methionine; PBMCs, peripheral blood mononuclear cells; PD-1, programmed cell death-1; PK, pharmacokinetic; PD-L1, programmed cell death-ligand 1; SAR, structure−activity relationship; SD, Sprague-Dawley; $t_{1/2}$, half-life; T_{max}, time of maximum plasma concentration; TCR, T cell receptor; TGI, tumor growth inhibition; TILs, tumor-infiltrating lymphocytes; TR-FRET, time-resolved fluorescence resonance energy transfer; Tyr, tyrosine; V_z, apparent distribution volume; XPhos Pd G2, XPhos palladacycle Gen. 2

■ REFERENCES

(1) Dong, H.; Strome, S. E.; Salomao, D. R.; Tamura, H.; Hirano, F.; Flies, D. B.; Roche, P. C.; Lu, J.; Zhu, G.; Tamada, K.; Lennon, V. A.; Celis, E.; Chen, L. Tumor-associated B7-H1 promotes T-cell apoptosis: A potential mechanism of immune evasion. *Nat. Med.* **2002**, *8*, 793−800.

(2) Zou, W.; Chen, L. Inhibitory B7-family molecules in the tumour microenvironment. *Nat. Rev. Immunol.* **2008**, *8*, 467−477.

(3) Greenwald, R. J.; Freeman, G. J.; Sharpe, A. H. The B7 family revisited. *Annu. Rev. Immunol.* **2005**, *23*, 515−548.

(4) Pardoll, D. M. The blockade of immune checkpoints in cancer immunotherapy. *Nat. Rev. Cancer* **2012**, *12*, 252−264.

(5) Mellman, I.; Coukos, G.; Dranoff, G. Cancer immunotherapy comes of age. *Nature* **2011**, *480*, 480−489.

(6) Ribas, A.; Wolchok, J. D. Cancer immunotherapy using checkpoint blockade. *Science* **2018**, *359*, 1350−1355.

(7) Topalian, S. L.; Drake, C. G.; Pardoll, D. M. Immune checkpoint blockade: a common denominator approach to cancer therapy. *Cancer Cell* **2015**, *27*, 450−461.

(8) Carvalho, S.; Levi-Schaffer, F.; Sela, M.; Yarden, Y. Immunotherapy of cancer: from monoclonal to oligoclonal cocktails of anti-cancer antibodies: IUPHAR Review 18. *Br. J. Pharmacol.* **2016**, *173*, 1407−1424.

(9) Robert, C.; Soria, J.-C.; Eggermont, A. M. M. Drug of the year: programmed death-1 receptor/programmed death-1 ligand-1 receptor monoclonal antibodies. *Eur. J. Canc.* **2013**, *49*, 2968−2971.

(10) Ledford, H.; Else, H.; Warren, M. Cancer immunologists scoop medicine Nobel prize. *Nature* **2018**, *562*, 20−21.

(11) Shinohara, T.; Taniwaki, M.; Ishida, Y.; Kawaichi, M.; Honjo, T. Structure and chromosomal localization of the human PD-1 gene (PDCD1). *Genomics* **1994**, *23*, 704−706.
(12) Agata, Y.; Kawasaki, A.; Nishimura, H.; Ishida, Y.; Tsubat, T.; Yagita, H.; Honjo, T. Expression of the PD-1 antigen on the surface of stimulated mouse T and B lymphocytes. *Int. Immunol.* **1996**, *8*, 765−772.
(13) Tumeh, P. C.; Harview, C. L.; Yearley, J. H.; Shintaku, I. P.; Taylor, E. J. M.; Robert, L.; Chmielowski, B.; Spasic, M.; Henry, G.; Ciobanu, V.; West, A. N.; Carmona, M.; Kivork, C.; Seja, E.; Cherry, G.; Gutierrez, A. J.; Grogan, T. R.; Mateus, C.; Tomasic, G.; Glaspy, J. A.; Emerson, R. O.; Robins, H.; Pierce, R. H.; Elashoff, D. A.; Robert, C.; Ribas, A. PD-1 blockade induces responses by inhibiting adaptive immune resistance. *Nature* **2014**, *515*, 568−571.
(14) Keir, M. E.; Butte, M. J.; Freeman, G. J.; Sharpe, A. H. PD-1 and its ligands in tolerance and immunity. *Annu. Rev. Immunol.* **2008**, *26*, 677−704.
(15) Hamanishi, J.; Mandai, M.; Iwasaki, M.; Okazaki, T.; Tanaka, Y.; Yamaguchi, K.; Higuchi, T.; Yagi, H.; Takakura, K.; Minato, N.; Honjo, T.; Fujii, S. Programmed cell death 1 ligand 1 and tumor-infiltrating CD8+ T lymphocytes are prognostic factors of human ovarian cancer. *Proc. Natl. Acad. Sci. U.S.A.* **2007**, *104*, 3360−3365.
(16) Tan, S.; Zhang, C. W.; Gao, G. F. Seeing is believing: anti-PD-1/PD-L1 monoclonal antibodies in action for checkpoint blockade tumor immunotherapy. *Signal Transduction Targeted Ther.* **2016**, *1*, 16029.
(17) Naidoo, J.; Page, D. B.; Li, B. T.; Connell, L. C.; Schindler, K.; Lacouture, M. E.; Postow, M. A.; Wolchok, J. D. Toxicities of the anti-PD-1 and anti-PD-L1 immune checkpoint antibodies. *Ann. Oncol.* **2015**, *26*, 2375−2391.
(18) Huck, B. R.; Kötzner, L.; Urbahns, K. Small molecules drive big improvements in immuno-oncology therapies. *Angew. Chem., Int. Ed. Engl.* **2018**, *57*, 4412−4428.
(19) Wang, T.; Wu, X.; Guo, C.; Zhang, K.; Xu, J.; Li, Z.; Jiang, S. Development of Inhibitors of the Programmed Cell Death-1/Programmed Cell Death-Ligand 1 Signaling Pathway. *J. Med. Chem.* **2019**, *62*, 1715−1730.
(20) Zak, K. M.; Kitel, R.; Przetocka, S.; Golik, P.; Guzik, K.; Musielak, B.; Dömling, A.; Dubin, G.; Holak, T. A. Structure of the complex of human programmed death 1, PD-1, and Its ligand PD-L1. *Structure* **2015**, *23*, 2341−2348.
(21) Guzik, K.; Zak, K. M.; Grudnik, P.; Magiera, K.; Musielak, B.; Törner, R.; Skalniak, L.; Dömling, A.; Dubin, G.; Holak, T. A. Small-molecule inhibitors of the programmed cell death-1/programmed death-ligand 1 (PD-1/PD-L1) interaction via transiently induced protein states and dimerization of PD-L1. *J. Med. Chem.* **2017**, *60*, 5857−5867.
(22) Skalniak, L.; Zak, K. M.; Guzik, K.; Magiera, K.; Musielak, B.; Pachota, M.; Szelazek, B.; Kocik, J.; Grudnik, P.; Tomala, M.; Krzanik, S.; Pyrc, K.; Dömling, A.; Dubin, G.; Holak, T. A. Small-molecule inhibitors of PD-1/PD-L1 immune checkpoint alleviate the PD-L1-induced exhaustion of T-cells. *Oncotarget* **2017**, *8*, 72167−72181.
(23) Konieczny, M.; Musielak, B.; Kocik, J.; Skalniak, L.; Sala, D.; Czub, M.; Magiera-Mularz, K.; Rodriguez, I.; Myrcha, M.; Stec, M.; Siedlar, M.; Holak, T. A.; Plewka, J. Di-bromo-Based Small-Molecule Inhibitors of the PD-1/PD-L1 Immune Checkpoint. *J. Med. Chem.* **2020**, *63*, 11271−11285.
(24) Basu, S.; Yang, J.; Xu, B.; Magiera-Mularz, K.; Skalniak, L.; Musielak, B.; Kholodovych, V.; Holak, T. A.; Hu, L. Design, Synthesis, Evaluation, and Structural Studies of C2-Symmetric Small Molecule Inhibitors of Programmed Cell Death-1/Programmed Death-Ligand 1 Protein-Protein Interaction. *J. Med. Chem.* **2019**, *62*, 7250−7263.
(25) Cheng, B.; Ren, Y.; Niu, X.; Wang, W.; Wang, S.; Tu, Y.; Liu, S.; Wang, J.; Yang, D.; Liao, G.; Chen, J. Discovery of Novel Resorcinol Dibenzyl Ethers Targeting the Programmed Cell Death-1/Programmed Cell Death-Ligand 1 Interaction as Potential Anticancer Agents. *J. Med. Chem.* **2020**, *63*, 8388−8358.
(26) Qin, M.; Cao, Q.; Zheng, S.; Tian, Y.; Zhang, H.; Xie, J.; Xie, H.; Liu, Y.; Zhao, Y.; Gong, P. Discovery of [1,2,4]Triazolo[4,3-a]pyridines as Potent Inhibitors Targeting the Programmed Cell Death-1/Programmed Cell Death-Ligand 1 Interaction. *J. Med. Chem.* **2019**, *62*, 4703−4715.
(27) Guo, J.; Luo, L.; Wang, Z.; Hu, N.; Wang, W.; Xie, F.; Liang, E.; Yan, X.; Xiao, J.; Li, S. Design, Synthesis, and Biological Evaluation of Linear Aliphatic Amine-Linked Triaryl Derivatives as Potent Small-Molecule Inhibitors of the Programmed Cell Death-1/Programmed Cell Death-Ligand 1 Interaction with Promising Antitumor Effects In Vivo. *J. Med. Chem.* **2020**, *63*, 13825−13850.
(28) Wang, Y.; Xu, Z.; Wu, T.; He, M.; Zhang, N. Aromatic Acetylene or Aromatic Ethylene Compound, Intermediate, Preparation Method, Pharmaceutical Composition and Use Thereof. WO2018006795A1, 2018.

https://doi.org/10.1021/acs.jmedchem.1c00010
J. Med. Chem. 2021, 64, 7390−7403